A Population Consequence of Acoustic Disturbance Model for Cuvier's beaked whale (*Ziphius cavirostris*) in Southern California
5 October 2018

David Moretti & Nancy DiMarzio
Naval Undersea Warfare Center Division
Code 70T Bldg 1351
1176 Howell St.
Newport RI 02842
phone: (401) 832-5749 fax: (401) 832-4396 email: david.moretti@navy.mil

Len Thomas & John Harwood
Centre for Research into Ecological and Environmental Modelling
The Observatory
University of St Andrews
St Andrews, Scotland KY16 9LZ
phone: +44 (1334) 461801 fax: +44 (1334) 461800 email: len.thomas@st-andrews.ac.uk

Erin Falcone & Greg Schorr
Marine Ecology and Telemetry Research
2420 Nellita Rd NW Seabeck WA 98380
phone: (206) 550-9806 email: efalcone@marecotel.org

Suggested reference: Moretti, D., DiMarzio, N., Thomas, L., Harwood, J., Schorr, G., and Falcone, E. 2018. A Population Consequence of Acoustic Disturbance Model for Cuvier's Beaked Whale (*Ziphius cavirostris*) in Southern California. Report Prepared for the Office of Naval Research, Award No. N0001415WX01677 / N000141512191 / N000141512899

Award Number: N0001415WX01677 / N000141512191 / N000141512899

TABLE OF CONTENTS

1.0 LONG-TERM GOALS

The project long-term goal is to create a Population Consequences of Acoustic Disturbance (PCAD) model for evaluating and monitoring the health of the Cuvier's beaked whale (*Ziphius cavirostris*, hereafter *Zc*) population on the U.S. Navy's Southern California Offshore Range (SCORE) in California with a focus on the possible population-level effect of mid-frequency active sonar (MFAS). The geographic focus within SCORE is the Southern California Anti-submarine warfare Range (SOAR) that includes an array of hydrophones that are used to monitor *Zc* vocalizations and sonar.

2.0 OBJECTIVES

The project extends the PCAD model created to describe the Blainville's beaked whale (*Mesoplodon densirostris*, hereafter *Md*) population at the Atlantic Undersea Test and Evaluation Center (AUTEC) to a new species (*Zc*) and location (SCORE) [1]. We have assembled the data required to parameterize the extended model using ship track and passive acoustic beaked whale data collected at SCORE, as well as photo-ID and satellite tag data collected in the same area by Marine Ecology and Telemetry Research.

One of the Navy's ultimate goals is to measure the "health of populations", rather than simply monitoring their size, especially those exposed to Mid-Frequency Active Sonar (MFAS). This program focuses directly on Cuvier's beaked whales, the "most sonar sensitive" species [2, 3]. This project combines visual, tag, biophysical, direct ship tracks and passive acoustic data to create a framework for evaluating the effect of repeated, long-term exposure to MFAS on a population of *Zc* on the Southern California Antisubmarine Warfare Range (SOAR) located off San Clemente Island in the San Nicolas Basin (Figure 1).

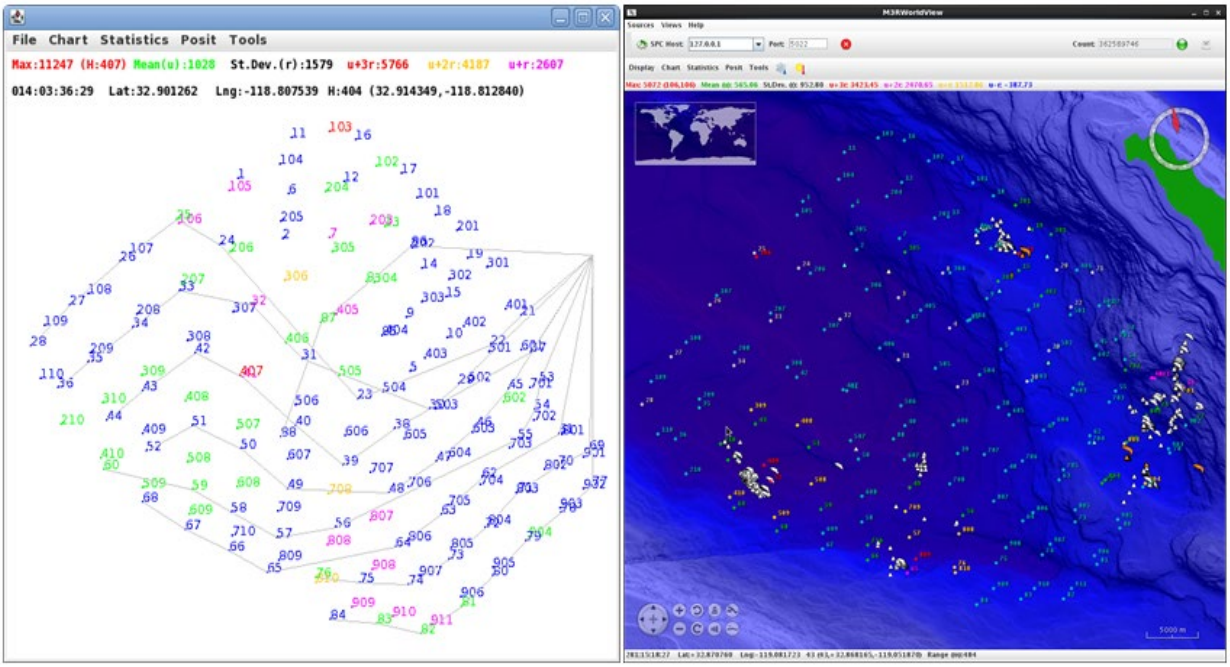

Figure 1. Marine Mammal Monitoring on Navy Ranges (M3R) system displays of odontocete localizations (right) on the Southern California Anti-submarine warfare Range (SOAR) off San Clemente Island. SOAR hydrophones are indicated by the numbers, with vocal activity on each phone indicated by color (left).

3.0APPROACH

3.1 Overview

The preponderance of past studies focused on the acute effect of MFAS exposure. However, on Navy ranges, animals also experience chronic exposure to MFAS from on-going operations over years. Estimating the cumulative effect of these repeated exposures and the resulting displacement is difficult. While understanding the acute effect of individual sonar exposures underpins this effort, understanding chronic effects requires many other inputs. These include an assessment of the local population, with estimates of the number of animals present, their temporal and spatial distribution, and the distribution of age/sex classes. It also requires estimates of life cycle parameters, such as gestational time, time to weaning, and calving intervals. Finally, it requires knowledge of MFAS use patterns and an understanding of behavioral reactions to MFAS on both an individual and population basis, particularly in terms of foraging [1].

To provide these data, a combination of data collection methods was employed that included passive acoustic monitoring, visual observations, deployment of tags that provided movement and dive data, photo-identification, and biopsy sampling.

These data were used to

1. estimate the abundance of animals present on SOAR,
2. assess the risk of behavioral disruption as a function of sonar exposure, and
3. investigate the effect of foraging dive disruption on population health.

3.2. Abundance

3.2.1 Base Statistics

Eight years of beaked whale detection data were collected on SOAR on a near continuous basis. The system primarily uses two types of detectors: a Fast Fourier Transform (FFT) based spectral energy detector ('Whdetect') [4] and a class-specific support vector machine (CS-SVM) classifier [5]. Table 1 shows the number of days per month on which archives with CS-SVM detections have been collected at SOAR between 2010 and 2017.

M3R SOAR Detection Archives												
	Jan	**Feb**	**Mar**	**Apr**	**May**	**Jun**	**Jul**	**Aug**	**Sep**	**Oct**	**Nov**	**Dec**
2010					7			9	30	29	22	23
2011	22	27	8	3	13		6	28	30	31	22	31
2012	27	23	18	30	15	6	1	4		17	13	10
2013					17	30	24	31	30	6	2	12
2014	31	22	28	29	28	17	14	17	28	14	4	31
2015	31	28	24	25	31	15	22	21	15	30	15	11
2016	31	27	31	25	18	7	16	31	27		26	22
2017	15		13	17	2		12	31	24	17	29	10+

Table 1. The number of days per month on which archives were collected at SOAR with the CS-SVM classifier. The CS-SVM *Zc* foraging click classifier was installed in May, 2010 (blue) and the CS-SVM *Zc* buzz click classifier was installed in July, 2014 (pink). FFT-based detections (Whdetect) have been collected at SOAR since 2006.

The analysis in this report focuses on 2015, which provided a near continuous data set across the entire year. To estimate abundance, CS-SVM detection reports were used to detect vocalizations from foraging beaked whales. These were used to isolate *Zc* foraging dive starts. The method described by Moretti et al. (2010) for *Md* at AUTEC was modified for *Zc* at SCORE [6].

The equation for animal abundance (N) presented by Moretti, et al. (2010) is:

$$N = sn_d/r_dT \qquad \textbf{Equation 1}$$

where:

n_d = total number of dive starts
s = average group size
r_d = dive rate (dives/unit time)
T = time period over which the measurement was made

For AUTEC is was assumed that the probability of detecting an *Md* dive start was 1.0 and the false alarm rate was 0.0. Given the hydrophone spacing at AUTEC (<4 km) and relative lack of interfering species, this was a reasonable approximation. However, the spacing of SOAR hydrophones approaches 5.0 km in the deepest section of the range. In addition, the number of interfering species, and their abundance, is significantly greater at SOAR. Several delphinid species are routinely detected, including Risso's dolphins (*Grampus griseus*), whose vocalization, based on analysis of data from the SOAR hydrophones, is similar to *Zc* in structure and frequency. Consequently, Equation1 was modified to include correction

factors for both the probability of detection (P_D) and the proportion (c) of false positives (false alarms).

$$\boldsymbol{N = n_d s(1 - c)/r_d T P_D} \qquad \textbf{Equation 2}$$

where:

n_d = total number of dive starts
s = average group size
r_d = dive rate (dives/unit time)
T = time period over which the measurement was made
c = proportion of false positives
P_D = probability of detection

Zc groups and their associated dive starts were extracted from binary archive files that contain detection reports from all detectors running on SOAR including the FFT and CS-SVM detection algorithms. CS-SVM reports were analyzed for *Zc* detections using two programs, Click Train Processor, that associated individual click detections into click trains, and Autogrouper (AG) that associated click trains into single Group Vocal Periods (GVPs).

The final output included the start and stop time of each GVP along with the hydrophones that detected the group and the number of clicks detected on each hydrophone. Based on a nominal click rate of 2 per second for an individual animal, the outputted groups were filtered to include only GVPs with between 300 (one individual for 5 minutes) and 43,200 (6 animals for 60 minutes) click detections. Also, the total GVP duration was limited to 90 minutes, which encompassed 99% (1133/1142) of foraging dive times reported by Schorr et al. (2014) [7].

To calculate the probability of detection and false alarm rate, 31 one-hour, systematic random samples were examined manually. The FFT detection reports were used to create 2D spectrograms that were reviewed by an analyst to determine if *Zc* GVPs occurred anywhere on SOAR. The start and stop times and group hydrophones were recorded. The results of each identified GVP were assigned one of three scores: high confidence (1), lower confidence (2) for groups that could be *Zc* with dolphins or possibly just dolphin clicks such as Risso's, and (3) Dolphins.

The results for these periods were then compared to the filtered Autogrouper output. Common groups were scored as "exact", "confused", "manual only" (false negative, hereafter FN), or "AG only" (false positive, hereafter FP). A group was considered an exact match if: (1) the groups had at least one hydrophone in common, (2) the hydrophones were not part of another group, and (3) the time periods overlapped. The "confused" matches occurred when all or some of the same hydrophones were identified by both the manual process and the AG program, and the time periods overlapped, but the number of groups and/or the hydrophone combinations forming the groups were not the same.

Detection statistics were then calculated from the 31 random samples. Correction factors were also calculated to derive the 'true' number of *Zc* group dive starts present from the number of AG groups detected. P_D was calculated as the number of dive starts correctly detected by the AG divided by the number of manually detected dive starts. The percentage of false negatives (dive starts missed by the AG) was the number of FNs divided by the number of manually detected dive starts, and the percentage of FPs (dive starts misidentified by the AG) was the number of FPs divided by the number of AG dive starts.

FP and FN correction factors for the AG dive start results were then derived as follows, using all samples combined:

1. The FP correction factor = 1 – (number of FP / number of AG dive starts)
2. The FN correction factor = 1 + (number of FN / (number of AG dive starts * FP correction factor)).

The detection statistics were considered for two cases: all group dive starts within the sample hour; and all group dive starts within the sample hour except "edge-only" cases. The "edge-only" cases are those groups that only contain hydrophones on the edge of the range. These are removed as it is likely that the associated group occurs outside the range boundary. If either the AG or the manual analysis reported an "edge-only" group, both this group and its matching group in the alternate method were removed from the analysis.

3.2.2 Hydrophone outages

Periods of hydrophone outages were identified in the data archives by isolating times when reports from hydrophones arranged on a physical hydrophone string were absent from the data archives. The hydrophone number is indicative of the array string where numbers in the 100s, 200s, 300s, etc. are associated with an individual physical hydrophone array. In total, there are nine hydrophone arrays of optically multiplexed hydrophones. Six combinations of string outages were observed (Table 2). To determine the effect of each outage combination, periods when all hydrophones were present were identified and the coincident GVPs tallied. For each year and outage combination, detection reports for missing hydrophones were removed from the results and the number of GVPs was recalculated. These results were then compared to the original all-hydrophone results to determine the change in GVP detection performance.

	2012	2013	2014	2015	2016	means	sums
Allhyd	1448	2190	7673	5899	7855	5013.00	25065
no100s	1177	1857	6591	5180	6996	4360.20	21801
no700s	1358	2057	7174	5449	7281	4663.80	23319
no900s	1367	2006	6935	5270	6999	4515.40	22577
no100s900s	1096	1673	5853	4551	6140	3862.60	19313
no100s600s700s	981	1561	5460	4204	5628	3566.80	17834
no600s_to_900s	1067	1511	4914	3501	4501	3098.80	15494

Table 2. Number of *Zc* groups detected for various Autogrouper configurations for the sample data from 2012-2016.

3.3 Risk function

SOAR includes 177 hydrophones that are distributed with approximately 4 km spacing at depths from 750 m to 1750 m (Figure 1). Each hydrophone is sampled at 96 kHz and the data is transmitted to shore where is it further processed or archived for later analysis. The data from 52 of these hydrophones was used in this analysis to estimate the potential response of *Zc* to sonar activity during 2015. Hydrophones on the southeast area of SCORE were excluded from the analysis because of known distribution patterns for *Zc* (Figure 6). Older

hydrophones that were not recently upgraded were excluded because they have since been replaced.

The M3R system was configured to automatically detect sonar activity and beaked whale vocalizations from the hydrophone data at SCORE [4]. Both the sonar detection and whale detector algorithms rely on the output from an FFT-based energy detector. This detector computes a set of 2048 point FFTs with 50% overlap and rectangular windows to obtain a frequency-domain signal with 46.875 Hz frequency resolution and 10.67 ms time resolution. The frequency domain signal is then converted to a binary valued signal by thresholding each sample against a time-varying background noise level.

The sonar detector algorithm implements an energy detector to identify sonar activity from the hydrophone data. The algorithm accepts the binary valued signal as its input and indicates that a sonar ping occurred whenever there are a sufficiently large number of positive samples in the binary signal on a single hydrophone within user defined time windows and frequency ranges. For each detection, the algorithm records the time, hydrophone, peak magnitude, and frequency bin corresponding to the peak magnitude. These detection reports were then passed through a heuristic, automated localization algorithm that attempted estimated the source position for each ping. The algorithm sequentially processed the sonar dataset and grouped individual detections between hydrophones into pings, then localized the source of each ping in time and space using hyperbolic multilateration that uses the time difference of arrival between hydrophones [8]. The grouping algorithm attempted to minimize an objective function that quantified the residual squared error between the predicted time of detection at each phone given the estimated source position with a sound speed of 1500 m/s and the observed time of detection. The algorithm was permitted to designate detections as ungrouped (false alarms) if the residual error from including the detection was sufficiently large and included a penalty term that ensured the algorithm would not simply choose the trivial optimization solution of designating all detections as ungrouped. After applying this procedure, a database of estimated sonar transmission time and positions was recorded for inclusion in the risk function analysis.

The second set of automated algorithms applied in this analysis identified *Zc* foraging vocalizations for the hydrophone data, grouped the vocalizations together into click trains, and associated click trains across hydrophones. The final output from these algorithms is a list of GVPs that are assumed to represent times when *Zc* are actively echolocating prey during a deep foraging dive. This output contains the ID of the hydrophones that detected each click train, the number of clicks in the click train, the start and end times, and the GVP to which the click trains belongs. The groups center was assumed to be the hydrophone with the highest click count. For this analysis, only click trains that were detected on at least 2 hydrophones and contained at least 500 clicks (approximately 3 minutes) were retained. Each GVP was then associated with the hydrophone that detected the greatest number of clicks.

The sonar and whale detection algorithms were used to process all data available from 2015, and these data were aggregated into 30 minute windows to estimate the risk function. For each 30 minute window when data were available, the total number of GVPs that started on each hydrophone was computed. The estimated maximum sound pressure level at each hydrophone's latitude and longitude, but at 100 m depth, was computed from the sonar dataset. This computation assumed that the sonar pings were transmitted at a nominal level of 215 dB re μPa @ 1m and that the total transmission loss may be modeled by $20\log_{10}(r)$,

where r is the horizontal distance from the estimated source position to the hydrophone in meters. This transmission loss model assumes spherical spreading and no sound attenuation, which is most valid for short ranges and likely to overestimate attenuation at long ranges. The risk function was then fitted as a generalized additive model (GAM) using a binomial family and a logit link function that estimated the presence of a GVP start within each time window as a function of the maximum received sonar level. The probability of disturbance from sonar exposure was estimated as 1 minus the predicted probability of GVP start from the GAM divided by the baseline probability of GVP start in the absence of sonar.

3.4 PCAD model parameters

3.4.1 Sonar and dive behavior

An estimate of the effect of MFAS operations on foraging dives on a daily basis over 2015 was undertaken. Days with sonar were identified using the FFT-based detection reports. Dive starts for each data-day were calculated as described above. The number of dives in the most recent preceding day with no MFAS was compared to the next most recent day with MFAS operations and the percentage "dive loss" calculated.

The number of groups present was calculated by dividing the total number of dive starts detected for each day by the mean dive-rate as calculated from tag studies [7]. The number of dives lost was estimated by multiplying the proportionate change in dives during MFAS operations by the mean number of dives per day derived from tags [7].

3.4.2 Population demographics

Zc photo-ID data were collected on and around SOAR from 2006 to 2017. During a typical sampling day, an RHIB with two expert observers was directed to vocalizing *Zc* by on-shore passive acoustic observers using the M3R system to monitor the SOAR hydrophones. The on-water team collected photos that were used to identify individuals and to assign those individuals to the appropriate age/sex class [9].

Females with dependent calves were noted in an attempt to determine life history stages. From these repeated observations age at sexual maturity, gestation time, and time to weaning were estimated [9]. An estimate of the ratio of dependent calves to adult females was derived, based on the number of animals assigned to each age/sex class.

3.5 *Zc* bioenergetics model

A generalized bioenergetics model for long-finned pilot whales (*Globicephala melas*) developed as part of the ONR-funded PCoD+ project (Developing widely-applicable models of the population consequences of disturbance) was adapted to model the energy requirements of different life-history stages of *Zc* and the potential effects of MFAS-related disturbance. The original pilot whale model is described in detail in the Appendix. The sonar and GVP detection data described in section 3.3 was used to estimate the probability that an individual Zc on SOAR during a particular 30 minute window would be disturbed, and the duration of that disturbance. This information was used to simulate disturbance histories for adult females of different ages to investigate how this might affect calf survival and inter-calf interval.

4.0 WORK COMPLETED

The following tasks have been completed:

1. Passive acoustic estimate of yearly/monthly *Zc* abundance on SOAR, corrected for the probability of detection, false alarm rate, and hydrophone outages;
2. Hydrophone calibration necessary for determining the received level from detection reports;
3. Detection of days when MFAS was active on SCORE during 2015;
4. Development of a preliminary *Zc* behavioral risk function
5. Analysis of field data for *Zc* population demographics including number of animals in different age/sex classes
6. Development of a preliminary PCAD model

5.0 RESULTS

5.1 Abundance

Data were obtained for dive starts from 2010 to 2017 using the semi-automatic tools described above. Autogrouper correction factors for the Probability of detection and the false alarm rate were measured (Table 3) along with correction factors for each combination of hydrophone outages (Table 4).

AutoGrouper case	n	Probability of Detection (PD)	% False Negative (FN)	% False Positive (FP)	Correction Factors	
					FP	FN
all groups	31	0.738	0.262	0.173	0.827	1.355
no edge only groups	31	0.759	0.241	0.185	0.815	1.318

Table 3. AutoGrouper detection statistics and correction factors for *Zc* in SOAR.

	2012	2013	2014	2015	2016	CF (Means)
no100s / allhyd	0.99	1.00	0.99	1.00	1.00	1.00
no700s / allhyd	1.00	0.99	0.99	0.99	0.98	0.99
no900s / allhyd	1.00	0.99	0.99	0.99	0.99	0.99
no100s900s / allhyd	0.99	0.99	0.98	0.99	1.00	0.99
no100s600s700s / allhyd	0.98	0.99	0.98	0.98	0.98	0.98
no600s_to_900s / allhyd	1.02	0.99	1.00	0.98	0.97	0.99

Table 4. Ratios of mean Group Vocal Periods (GVPs) for the various Autogrouper configurations to the Autogrouper run with all hydrophones. CF (the means of the ratios across years 2012 – 2016) indicates the correction factors derived for the GVPs.

The yearly data were combined and corrected for detection statistics and hydrophone outages to provide a mean monthly estimate of abundance across SOAR (Figure 2 and 3).

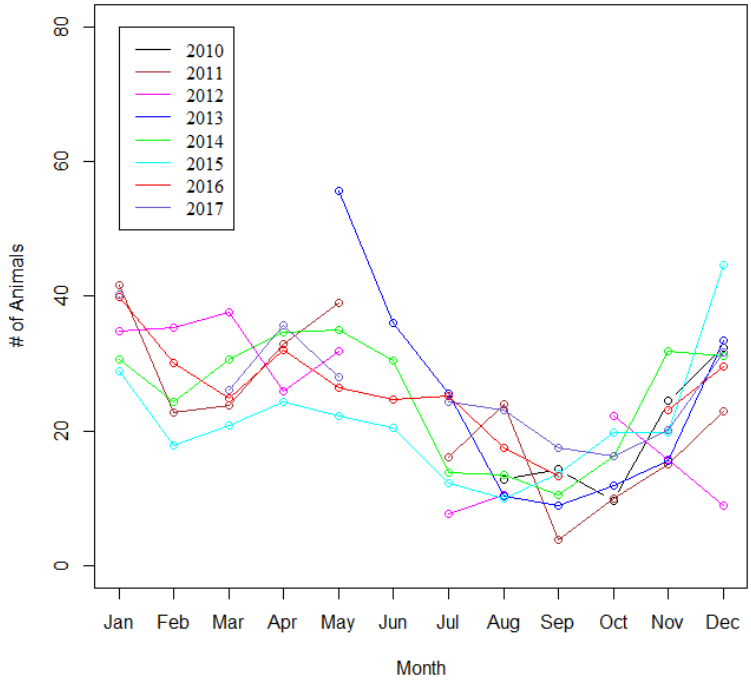

Figure 2. Corrected mean monthly *Zc* abundance for the years 2010-2017.

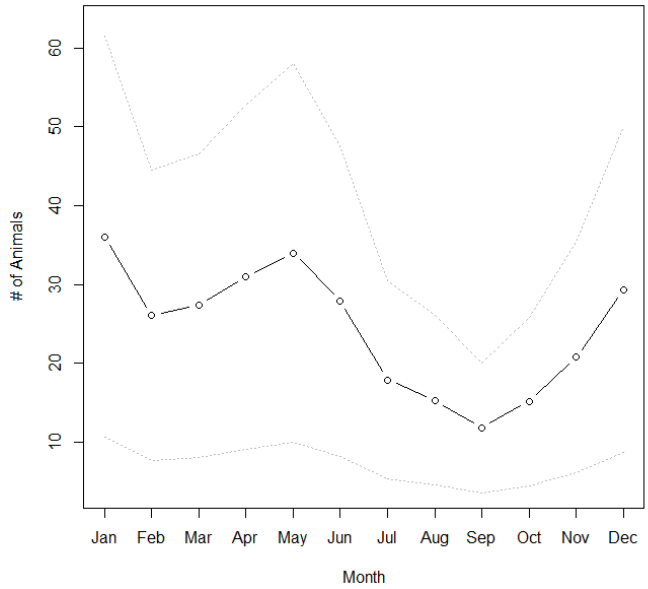

Figure 3. Corrected mean monthly *Zc* abundance at SOAR, averaged across all years.

	Jan	Feb	Mar	Apr	May	Jun	Jul	Aug	Sep	Oct	Nov	Dec
2010	NA	NA	NA	NA	NA	NA	NA	12.88	14.33	9.61	24.45	32.42
2011	41.72	22.83	23.79	32.85	39.10	NA	16.18	24.05	3.89	9.97	15.03	22.97
2012	34.86	35.35	37.65	25.98	31.78	NA	7.65	10.59	NA	22.21	15.82	9.02
2013	NA	NA	NA	NA	55.55	36.12	25.65	10.38	8.93	11.94	15.69	33.38
2014	30.70	24.36	30.70	34.73	34.92	30.46	13.78	13.49	10.60	16.33	31.78	31.10
2015	28.90	17.81	20.79	24.29	22.22	20.50	12.33	10.03	13.67	19.76	19.73	44.66
2016	39.86	30.18	24.88	32.08	26.36	24.68	25.19	17.55	13.37	NA	23.20	29.53
2017	40.21	NA	26.15	35.78	28.05	NA	24.42	23.03	17.55	16.35	20.15	31.70

Table 5. Mean monthly *Zc* abundance on SOAR for 2010 - 2017. NAs indicate periods without data.

Data from the month of December were available from each year of the study (Table 5), and these data were used to investige trends in abundance (Figure 4).

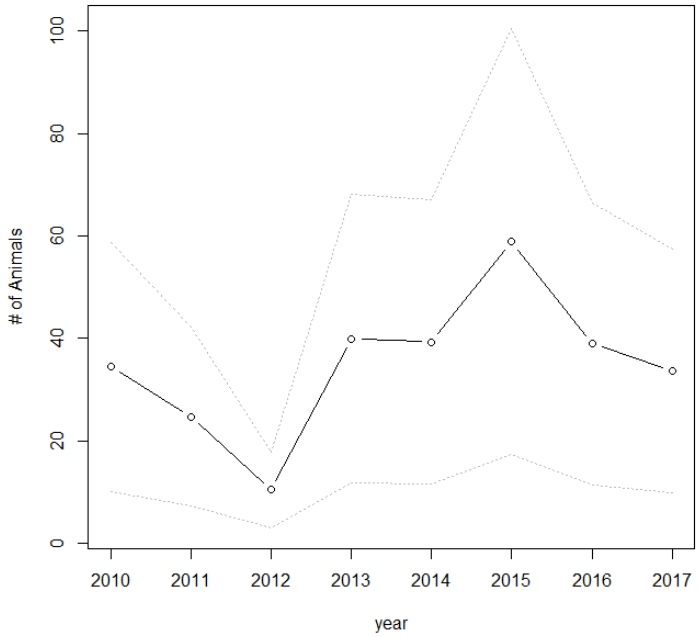

Figure 4. Corrected mean monthly *Zc* abundance for the month of December, 2010-2017.

Data for each year were also analyzed for changes on a daily basis, this suggested that there is a diurnal pattern of variation in the number of GVPs detected on SOAR (Figure 5) .

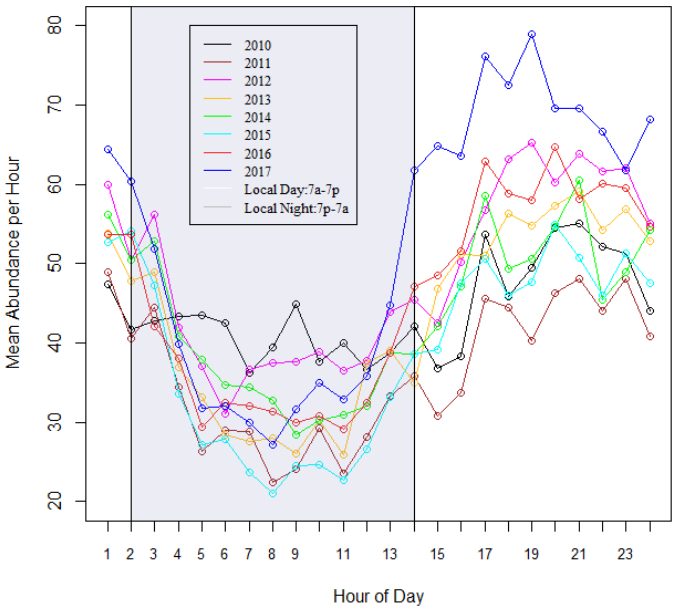

Figure 5. Mean *Zc* abundance per hour on a 24-hour cycle. Note that the times are in UTC, and the gray shaded area indicates the approximate local night hours, if local day is considered 7am to 7pm, and local night is considered 7pm to 7am. There is a 7 or 8-hour difference between local time on San Clemente Island and UTC, depending on Daylight Savings Time.

5.2 Risk function

Data were available for 12,014 of the 17,520 30 minute time windows during 2015. At least 1 GVP start was recorded during 4,775 of these time windows (Figure 6). The GVP starts and sonar pings were distributed throughout the full year of sampling, and the data do not appear to show any seasonal trends (Figure 7). The fitted GAM predicted that the probability of a GVP start declined as the received sonar level increased (Figure 8): the baseline probability of a GVP start on a randomly chosen hydrophone in the absence of sonar is approximately 0.01, and this value declines an order of magnitude as the sonar exposure level increases. The risk function computed from this fit indicates that there is a 50% probability of disturbance at a received level of 130 dB re µPa (Figure 9). This implies an attenuation loss of approximately 85 dB from the nominal source level, which would occur at a range of approximately 18 km. At this range, spreading is likely to have transitioned to a cylindrical spreading scenario, where absorption and refraction may become important, so the actual sonar exposure levels may differ from the estimated values. Therefore, this risk function should be interpreted with care and viewed as a preliminary result until the exposure levels can be confirmed from observational data or better estimated.

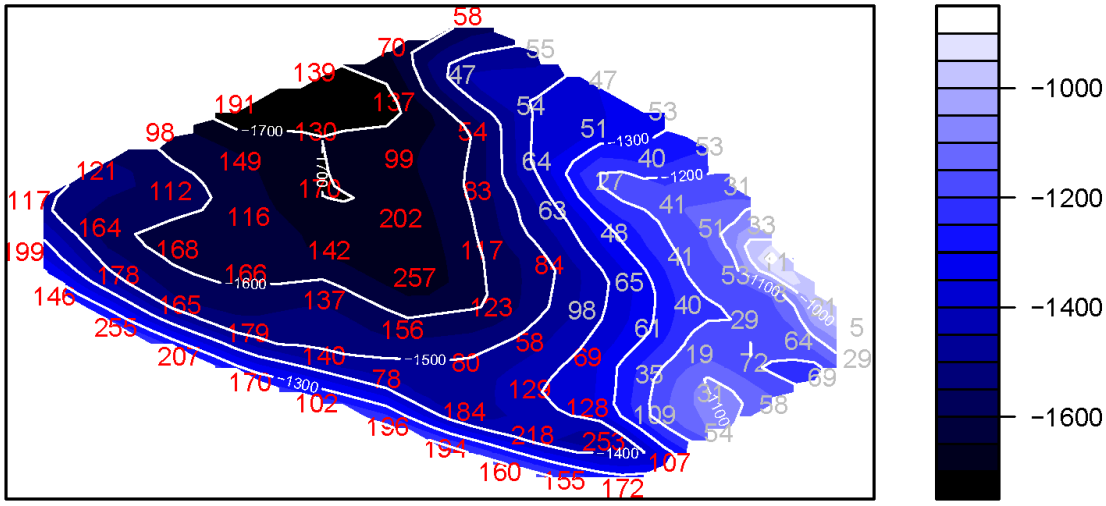

Figure 6. The total number of GVP starts on each hydrophone is overlaid on the bathymetry of the SCORE range. The GVP start counts are indicated in red for hydrophones that are included in this analysis and grey for hydrophones that are excluded, and are plotted at the location of each hydrophone. The background colors and contours indicate water depth in meters as estimated by the hydrophone depths.

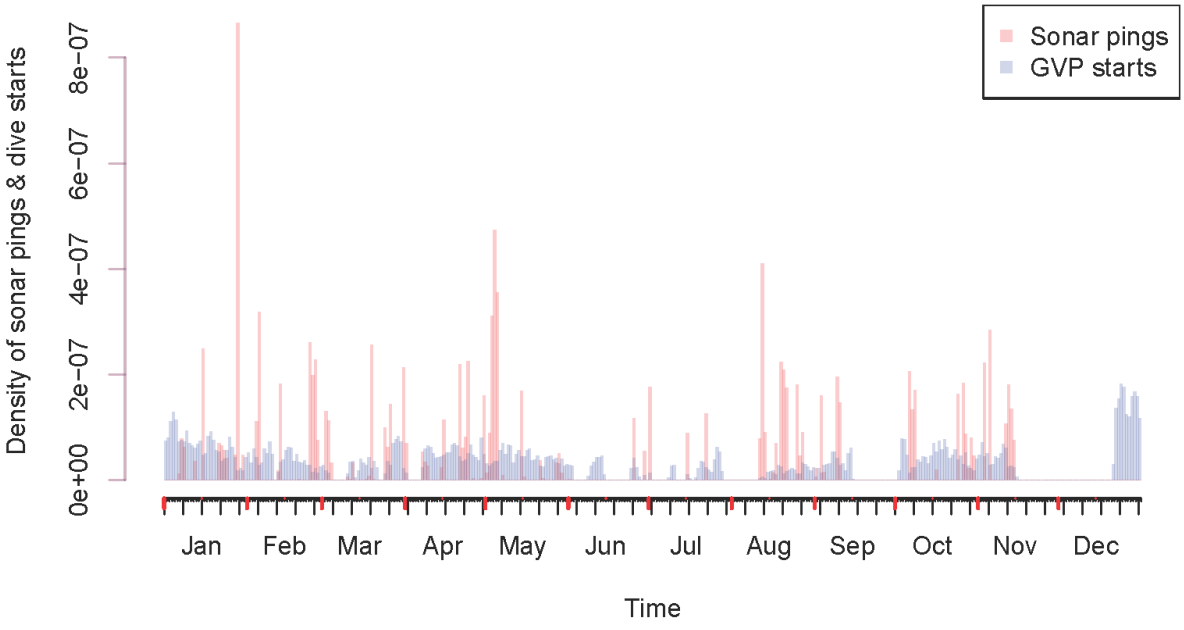

Figure 7. The number of sonar pings (red) and GVP starts (blue) is indicated for each day of the year (2015).

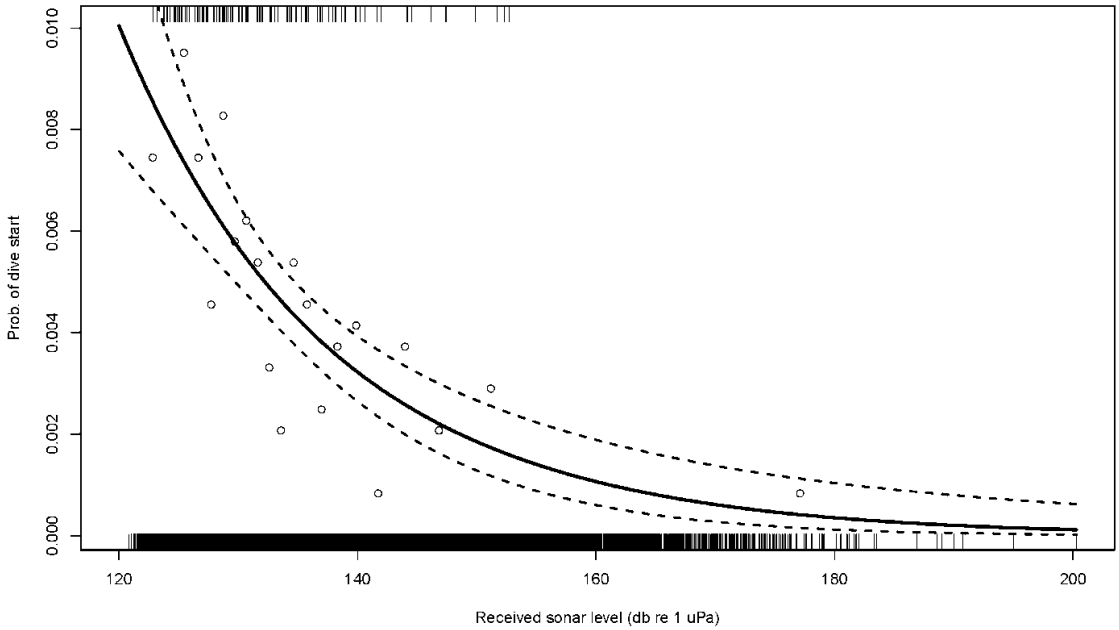

Figure 8. The probability of a GVP start during a time window-hydrophone pair is plotted along with a GAM fit to the data. The received sonar level was estimated at 100 m depth. Each circle indicates the mean GVP start probability for 5% of the data, the solid black line indicates a GAM fit as indicated in the text, and the dashed lines indicate 95% confidence intervals for the GAM.

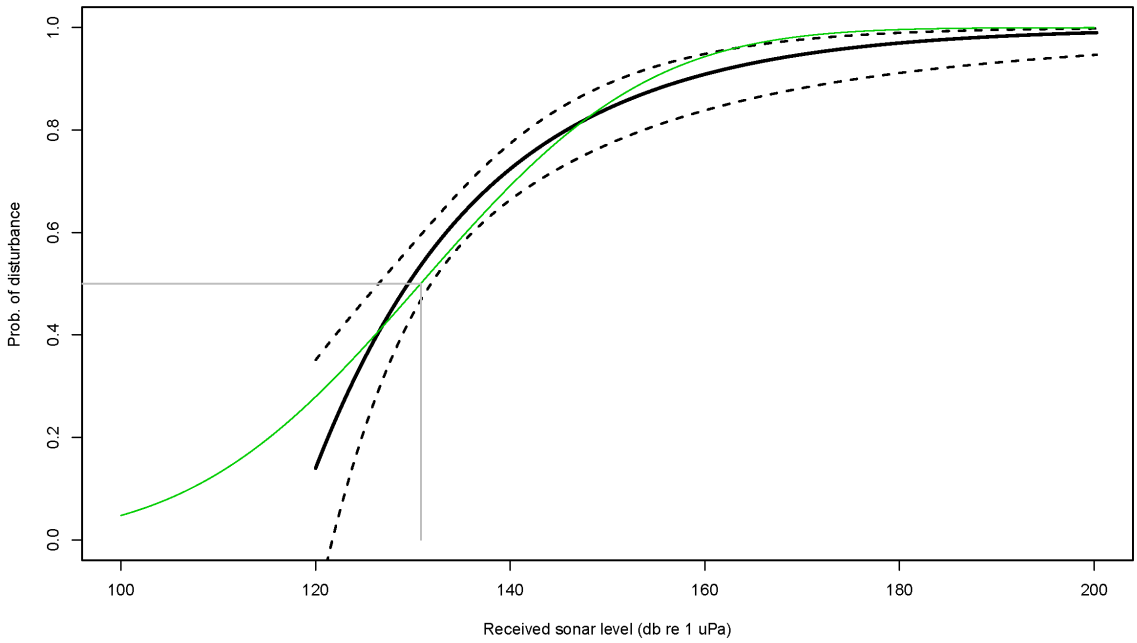

Figure 9. The probability of foraging disturbance due to sonar exposure is plotted as a function of the sonar exposure level. The black solid and dashed lines indicate the estimated values from the GAM fit to predict the probability of a GVP start as a function of sonar exposure level. The green line is a GLM fit to the same data, and the grey lines indicate the 50% probability of disturbance level based on the GLM fit.

5.3 Sonar and dive behavior

Changes in the number of *Zc* dive starts on SOAR in relation to MFAS operations was documented. *Zc* dive starts were extracted from the data archives along with MFAS received levels on the surrounding hydrophones (Figure 10).

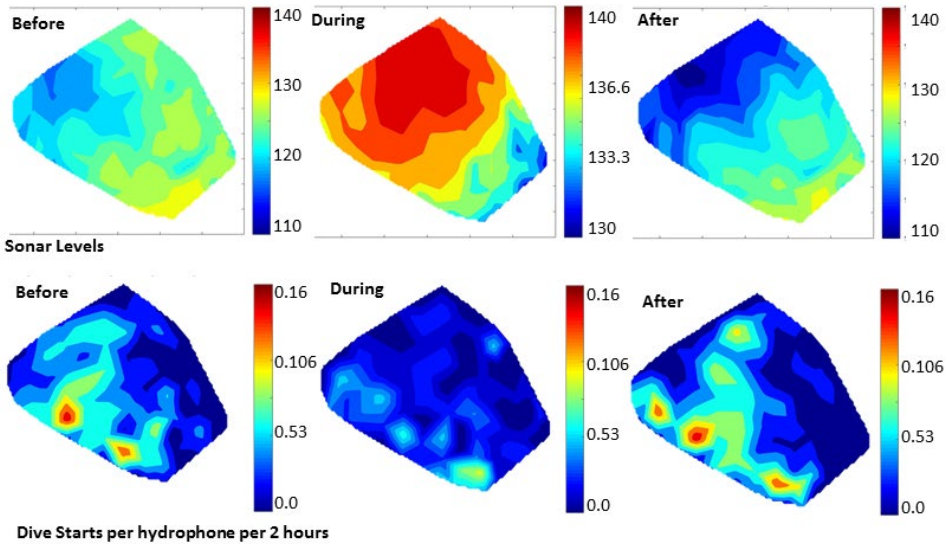

Figure 10. Sound field (dB re µPa) derived from hydrophone measurements the day before, during, and after a surface ship MFAS operation (upper panels) versus mean dive starts (2 hr periods) derived from hydrophone measurements on SOAR before, during, and after a surface ship operation (lower panels).

Days with MFAS operations were identified in the data based on the detection of sonar pings for years 2010 to 2017 along with the number of corresponding *Zc* dive starts on a daily basis. The number of dive starts for each day with MFAS operations was divided by the number of dive starts on the most recent day with no MFAS preceding the operation An example of the results are given in Table 6.

Year	15	16	17	18	19	20	21	22	23	24	25	26	27	28	29	30
2010	NA	NA	NA	NA	NA	NA	NA	NA	NA	NA	NA	NA	NA	NA	NA	NA
2011	NA	0.65	NA	0.93	0.64	0.73	0.90	NA	NA	1.35	NA	NA	NA	NA	NA	NA
2012	NA	NA	NA	NA	NA	NA	NA	NA	NA	NA	0.70	0.33	NA	NA	NA	NA
2013	NA	NA	NA	NA	NA	NA	NA	NA	NA	NA	NA	NA	NA	NA	NA	NA
2014	0.66	0.45	0.34	NA	NA	0.68	0.61	0.57	0.29	NA	0.94	NA	0.65	NA	NA	1.12
2015	0.69	0.72	NA	NA	NA	0.91	0.82	0.57	0.46	0.55	0.76	0.81	0.54	0.19	0.41	0.28
2016	1.03	NA	NA	NA	1.19	NA	NA	0.60	NA	NA	0.67	0.67	0.68	0.66	NA	NA
2017	NA	NA	NA	NA	NA	NA	NA	NA	NA	NA	NA	NA	NA	NA	NA	NA

Table 6. The proportion of dive starts per day for day 15 through 30 out of 365 days (366 days for 2012, 2016). Days with no MFAS transmissions are listed as "NA"

5.4 Population demographics

Two hundred unique individuals were photographed in 322 total identifications. Of the 200 individuals, 184 were assigned to age classes and 149 were assigned to sex classes (83 female and 66 males). Twenty-one mother-calf pairs were sighted over the study. The longest separation between subsequent sightings of the same mother-calf pair was 734 days (2 years and 4 days) [9].

Five females and five males transitioned through age classes. Based on the sighting history and physical appearance, it is estimated that females begin to sexually mature at approximately age seven and transition to adulthood by approximately age ten [9].

Of the 184 individuals assigned to an age class with any level of confidence (High, Medium, Low), 120 were classed as adults (56%), 29 as sub-adults (14%), 13 as juveniles (6%), and 22 as calves (10%), at their most recent sighting. In total 73 individuals were classed as adult females [9].

Note, the probability of being marked may depend on age, so that animals that are older are more likely to be uniquely marked and so identified. This could cause a bias in these numbers relative to the population numbers. Also, different age classes may be differentially detectable which would also cause a bias.

5.5 Bioenergetics modelling

Analysis of data from the 12,014 30 minute time windows for which hydrophone data were available during 2015 indicated that 59% fewer GVPs were detected in time windows when sonar was also detected compared with time windows when no sonar was detected. It took around 3 hours for GVP detection rates to recover to close to pre-exposure levels. Time windows that included a sonar detection and which were within 3 hours of each other were amalgamated into disturbance events. We assumed that a *Zc* individual that was disturbed during one of these events did not feed. The average duration of these events was 6.6 hours, although they ranged from 3 hours to 34 hours. The predicted effect of these disturbance events depended on what assumption were made about the productivity of the benthic environment on SOAR and what proportion of time individual *Zc* spent on the range. If the productivity of the environment was set to a level that allowed females as young as eight years to raise offspring successfully (as suggested by [11]) and females spend all of their time on the range, current levels of disturbance on SOAR are likely to lead to the death of most calves as a result of insufficient milk supply by their mothers. However, results from the population demographics study (section 4.3) clearly indicate this is not the case. Increasing the productivity of the environment by 10% was sufficient to allow all females aged 10 and over to raise young successfully, as has been observed. The bioenergetics model makes a number of predictions about the effects of disturbance on *Zc* behavior and body condition which will be compared to observations of tagged animals on the range to evaluate its credibility.

6.0 IMPACT/APPLICATION

The tools and data provided by this program, in particular the estimate of *Zc* abundance and the behavioral risk function, will inform the Navy's environmental compliance requirements including the statistical modelling as to the effect of MFAS operations on *Zc*.

Ultimately, the PCAD model for *Zc* will aid in regulatory decisions as to the effect of repeated sonar use on the local population, provided the necessary information required to calibrate the model are elucidated.

7.0 TRANSITIONS

To address Federal environmental laws including the Marine Mammal Protection Act (MMPA) and the Endangered Species Acts (ESA) the Navy has initiated the Integrated Comprehensive Monitoring Program (ICMP). The ICMP provides the framework for Navy monitoring on range complexes within direct U.S. legal jurisdiction.

The proposal directly addresses the ICMP stated goal of providing "*An increase in our understanding of how anticipated adverse effects on individual animals may impact the population, species, or stock (specifically through effects on annual rates of recruitment or survival)*." In addition, it will both inform and affect the remaining goals listed below.

An increase in the probability of detecting marine mammals and other threatened or endangered marine species, both within the safety zone (thus allowing for more effective implementation of the mitigation) and in general to generate more data to contribute to the effects analyses.
An increase in our understanding of how many marine mammals and other threatened or endangered marine species are likely to be exposed to levels of Mid-Frequency Active Sonar (MFAS), High-Frequency Active Sonar (HFAS), underwater detonations, or other stimuli that are associated with specific adverse effects, such as behavioral harassment, Temporary Threshold Shift (TTS), or Permanent Threshold Shift (PTS).
An increase in our understanding of how marine mammals and other threatened or endangered marine species respond (behaviorally or physiologically) to MFAS/HFAS, underwater detonations, or other stimuli at specific received levels that result in the anticipated take of individual animals.
An increase in our understanding of the effectiveness of certain mitigation and monitoring measures.
A better understanding and record of the manner in which the authorized entity complies with the incidental take authorization

This program will provide input on an annual basis through the ICMP annual Adaptive Management Review (AMR). This provides a mechanism to incorporate evolving technology developed through this program into the Navy's monitoring program without waiting to the end of the proposed 5-year schedule. This is particularly important as based on preliminary

M3R results from AUTEC, where *Md* avoids sonar but at levels significantly lower than suggested by the current dose response function.

8.0 RELATED PROJECTS

PCoD Lite - Using an Interim PCoD Protocol to Assess the Effects of Disturbance Associated with US Navy Exercises on Marine Mammal Populations
Office of Naval Research (ONR)
Principal Investigator: Cormac Booth, Mark Burgman, Carl Donovan, John Harwood, Len Thomas, Robert Schick, Jason Wood
The objective of the project was to illustrate how the interim PCoD protocol can be used to inform the process of determining whether or not Navy activities are likely to have an impact on populations of two priority species at two different Navy ranges within the regulatory frameworks associated with the Marine Mammal Protection Act (MMPA) and Endangered Species Act (ESA).

Population Parameters of Blainville´s and Cuvier´s Beaked Whales
Office of Naval Research (ONR)
Principal Investigator: Natacha Aguilar, Phil Hammond, Cristina Reyes, Agustina Schiavi
This project continues a long-term photo-ID study started in the Canary Islands in 2003 in order to obtain a sufficient sample size for demographic modeling.

Measuring the Effect of Range on the Behavioral Response of Marine Mammals Through the Use of Navy Sonar (Project #LMR-30)
Living Marine Resources Program (LMR)
Principal Investigator: Stephanie Watwood
To assess the effect of sonar source sources and distance (range), researchers are conducting controlled exposure experiments (CEE) with sonar from two different platforms. Each will be deployed at multiple, pre-defined distances from tagged animals to collect data on responses.

Cuvier's Beaked Whale and Fin Whale Behavior During Military Sonar Operations: Using Medium-term Tag Technology to Develop Empirical Risk Functions (Project #LMR-23)
Living Marine Resources Program (LMR)
Principal Investigators: Greg Schorr, Erin Falcone
The effort will generate significantly larger samples of high-resolution behavioral data, particularly for beaked whales, to support development of risk functions.

A Blainville's Beaked Whale Behavioral Risk Function for Hawaiian Populations (Project #LMR-25)
Living Marine Resources Program (LMR)
Principal Investigators: David Moretti, Len Thomas
This effort will result in the publication of the first behavioral risk function for the Blainville's beaked whale at the Pacific Missile Range Facility.

SOCAL Behavioral Response Study (Project #LMR-2)
Living Marine Resources Program (LMR)
Principal Investigator: John Calambokidis and Brandon Southall
This project is designed to increase understanding of marine mammal reactions to sound and provide a more robust scientific basis for estimating the effect of Navy mid-frequency active sonar (MFAS) on marine mammal behavior. Project co-funded by ONR and SERDP.

Demographics and diving behavior of Cuvier's beaked whales at Guadalupe Island, Mexico: A comparative study to better understand sonar impacts at SCORE.
Office of Naval Research (ONR)
Principal Investigator: Gregory Schorr
The goal of this project is to provide a comparative site to SOAR for *Zc* diving behavior and populaiton demographis in an area of no MFAS disturbance.

PCoD+: Developing widely-applicable models of the population consequences of disturbance
Office of Naval Research (ONR)
Principal Investigators: Cormac Booth & John Harwood
The goal of this project is to overcome existing impediments to the full implementation of the PCoD framework.

Integrated Measurement of Naval Sonar Operations and Precise Cetacean Locations: Integration of Fastloc GPS into a LIMPET tag.
Strategic Environmental Science and Technology Program (ESTCP)
The objective of this project was to 1.) develop and implement a sonar detection algorithm on each of the Navy's undersea ranges and 2.) integrate GPS into a tag that can be used to more precisely monitor the movement of cetaceans with and without sonar present.

9.0 REFERENCES

[1] L. F. New, Moretti, David J., Hooker, Sascha K. and Simmons, Samantha E., "Using energetic models to investigate the survival and reproduction of beaked whales (family Ziphiidae)," *PLoS One,* 2013.

[2] A. D'Amico, R. Gisiner, D. Ketten, J. Hammock, C. Johnson, P. Tyack and J. Mead, "Beaked whale strandings and naval exercises," *Aquatic Mammals,* vol. 35(4), pp. 435-444, 2009.

[3] R. Filadelfo, J. Mintz, E. Michlovich, A. D'Amico, P. Tyack and D. Ketten, "Correlating military sonar use with beaked whale mass strandings: What do the historical data show?," *Aquatic Mammals,* vol. 35(4), pp. 445-451, 2009.

[4] S. M. Jarvis, R. P. Morrissey, D. J. Moretti and J. A. Shaffer, "Detection, Localization, and Monitoring of Marine Mammals in Open Ocean Environments using Fields of Spaced Bottom Mounted Hydrophones," *Marine Technology Society Journal,* vol. 48, no. 1, pp. 5-20, Feb. 2014.

[5] S. Jarvis, *A Novel Method for Multi-Class Classification Using Support Vector Machines,* 2012.

[6] D. Moretti, T. Marques, L. Thomas, N. DiMarzio, A. Dilley, R. Morrissey, E. McCarthy, J. Ward and S. Jarvis, "A dive counting density estimation method for Blainville's beaked whale (Mesoplodon densirostris) using a bottom-mounted hydrophone field as applied to a Mid-Frequency Active (MFA) sonar operation," *J. Applied Acoustics,* vol. 71(11), pp. 1036-1042, 2010.

[7] G. S. Schorr, E. A. Falcone, D. J. Moretti and R. D. Andrews, "First Long-Term Behavioral Records from Cuvier's Beaked Whales (Ziphius cavirostris) Reveal Record-Breaking Dives," *PLoS ONE ,* vol. 9, no. 3, March 2014.

[8] H. Vincent, *Models, algorithms, and measurements for underwater acoustic positioning,* 2001.

[9] E. A. Falcone, E. L. Keene and G. S. Schorr, *A population consequence of acoustic disturbance model for Cuvier's beaked whale ("Ziphius cavirostris") in Southern California: Photo-ID and Tag Data Components,* Seabeck, WA: Marine Ecology and Telemetry Research, 2017.

[10] C. G. Booth, C. Donovon, R. Plunkett and J. Harwood, "Using and interim protocol to assess the effects of disturbance associated with U.S. Navy exercises on marine mammal populations: Interim Report Report Code SMRUC-ONR-2016-004, Submitted to the Offis o fnaval Research - Marine Mammal & Biology Program," February 2016.

[11] J.G. Mead, "Survey of Reproductive Data for the Beaked Whales (Ziphiidae)". Report of the International Whaling Commission Special Issue 6, pp. 91-96. Cambridge 1984.

10.0 AWARDS

Marine Mammal Monitoring on Navy Ranges (M3R) National Association of Environmental Professionals 2018 National Enviromental Excellence Award for *Best Available Environmental Technology*

11.0 APPENDIX

Technical Report
ONR BAA N00014-16-R-BA01

A Population Consequence of Acoustic Disturbance Model for Cuvier's beaked whale (*Ziphius cavirostris*) in Southern California: Bioenergetics Model

September 2018

John Harwood
Centre for Research into Ecological and Environmental Modelling, University of St Andrews, St Andrews, Fife KY16 9LZ, UK
jh17@st-andrews.ac.uk
David Moretti
Naval Undersea Warfare Center Division
Code 70T Bldg 1351
1176 Howell St.
Newport RI 02842

1. Introduction

Tagging studies of Cuvier's beaked whales (*Ziphius cavirostris* - henceforth *Zc*) exposed to multi-frequency active sonar (MFAS) on the Southern California Anti-submarine Warfare Range (SOAR) have revealed changes in behavior - in particular an increase in the interval between deep dives - that could disrupt foraging and affect individual fitness (Falcone et al., 2017). In this report, we describe the development of a Dynamic Energy Budget (DEB) model for *Zc* that can be used to assess the potential effects of MFAS exposure on individual energy budgets and key demographic rates (particularly calf survival and inter-calf interval).

2. Bioenergetics model description

We modified a DEB model for the North Atlantic population of long-finned pilot whales (*Globicephala melas*) developed by Hin et al. as part of the ONR-funded PCoD+ project, to make it applicable to *Zc*. A detailed description of the pilot whale model is provided in Annex A. The pilot whale DEB model describes the way in which the life history processes (growth, reproduction and survival) of a female and her calves depend on the way in which assimilated energy is allocated between different processes (Lockyer 2007; Kooijman 2010; Lika and Kooijman 2011). Energy can temporarily be stored in a reserve compartment, which functions as a buffer between incoming and outgoing energy flows (De Roos et al. 2009).

This reserve compartment is mainly stored internally (in and around visceral organs and muscle), but also in blubber (Lockyer 1993; 2007), and can be mobilized to serve energetic needs. The size of this reserve controls various life history functions (Lockyer 2007; Miller et al. 2011), and therefore links the effects of disturbance and environmental conditions to survival and reproduction. To control for differences in absolute size during ontogeny, Hin et al. used 'body condition' (reserve mass over total body mass) as a measure of individual health. A good body condition is required for successful calf recruitment (pregnancy and

lactation) and a poor body condition compromises survival and decreases life expectancy. We set an upper limit (0.3) on body condition, to reflect the fact that deep diving cetaceans probably try to maintain neutral, or slightly negative, buoyancy (Aoki, Sato, Isojunno, Narazaki, & Miller, 2017).

The model requires a growth curve that specifies length at age. We followed Hin et al. by using a von Bertalanffy growth curve, with a length at birth (L_0) of 270 cm and a maximum length (L_∞) of 754 cm, both taken from Mead (1984). The growth rate was then adjusted so that the mean length at first breeding (580 cm) proposed by Mead (1984) was attained at an age of 6 years. We used the relationship between length and body mass for northern bottlenose whales used by New, Moretti, Hooker, Costa, & Simmons (2013) for all beaked whales to calculate core body mass at age.
Environmental productivity is modelled by a variable *R* (resource density) that represents the maximum potential assimilated energy provided by prey in the local environment (i.e. we do not model prey energy density or digestibility explicitly). Actual energy intake is determined by an individual's body size (large individuals can consume more than small ones), and its body condition (individuals that are close to the maximum permitted body condition consume less than those that are in poor condition). This allows individuals to compensate for the effects of disturbance on foraging by consuming more prey in subsequent foraging bouts.

Mothers and their calves are at risk of mortality from starvation if their body condition falls below a predefined threshold level (0.15 in this case). Mortality increases with declining body condition according to a hyperbolic function, with the speed of increase controlled by parameter μ_s (De Roos et al. 2009). We assumed that a sexually mature female would only become pregnant if the total energy content of her reserves was greater than the sum of the threshold for starvation mortality plus the costs of growing a fetus to term. Following Mead (1984), we assumed that the gestation period was 1 year.

The duration of lactation was set at 2 years, based on the observations of Falcone et al. (this report), but we assumed that the proportion of the calf's energy requirement provided by its mother decreases steadily after the first year. A calf's foraging ability was assumed to increase steadily with age, although adult feeding efficiency is not attained until age 5. The calf's demand for milk is determined by its size and body condition. Females are assumed to meet all of this demand when they are in good body condition, but to reduce milk supply if their body condition approaches the threshold for starvation-related mortality.
Hin et al. modelled the effects of disturbance over the entire lifetime of a female pilot whale. However, this requires information on age-specific mortality rates, which is not available for *Zc*. We therefore focussed on the effects of disturbance over a single reproductive cycle, from the start of one pregnancy to the start of the next pregnancy, for females of different ages (and therefore sizes).

Initially, we set *R* at a level such that it was just possible for a female that became pregnant at age 8 years to raise a calf successfully (Fig. 2).

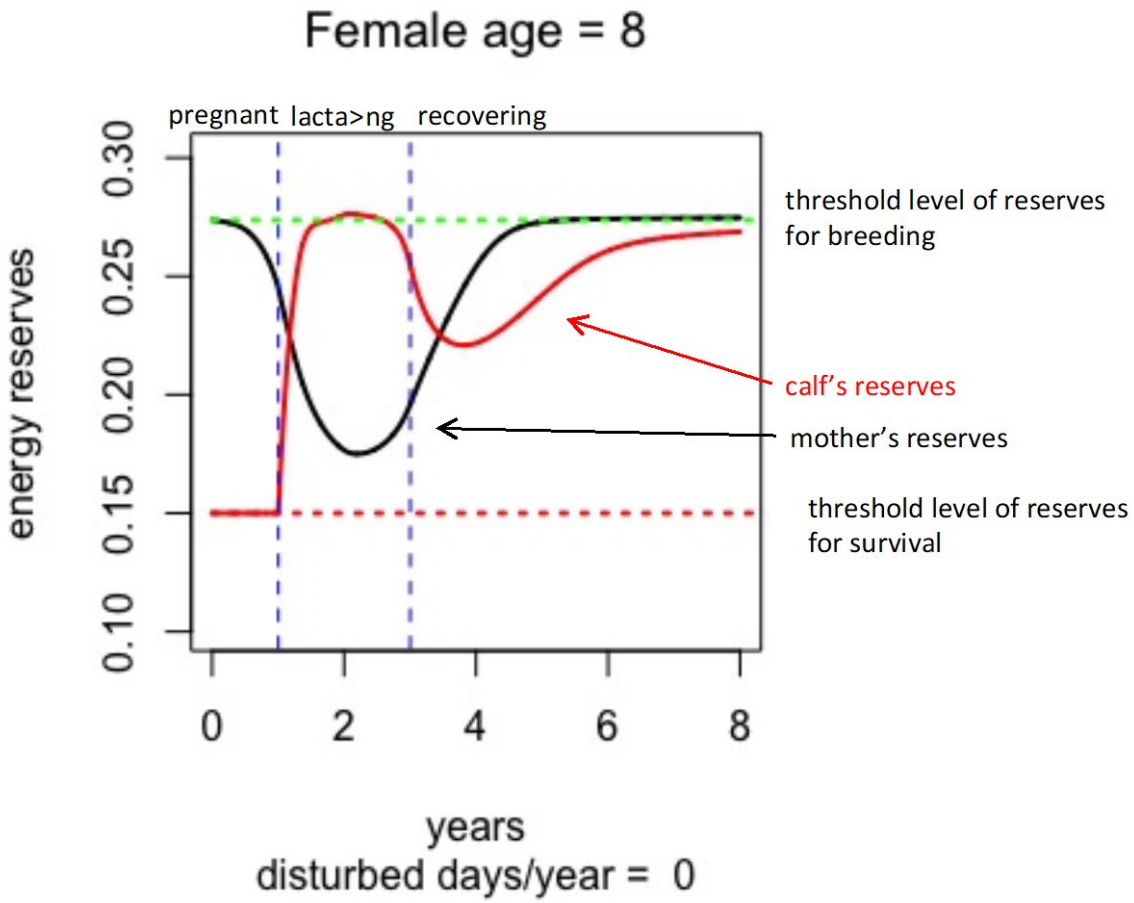

Figure 1. Predicted changes over time in the body condition of an 8 year-old female Zc and her calf over the course of pregnancy and lactation. This female would have an inter-calf interval of 6 years if she became pregnancy as soon as her body condition reached the threshold for reproduction (5 years after the start of the previous pregnancy).

3. Modelling exposure to MFAS on SOAR and its effect on energy intake

The sonar and Group Vocalization Period (GVP) detection data described in section 3.3 of Moretti et al. (this report) was used to estimate the probability that an individual *Zc* on SOAR during a particular 30 minute window would be disturbed, and the duration of that disturbance. Analysis of data from the 12,014 30 minute time windows for which hydrophone data were available during 2015 indicated that the mean number of GVPs detected in time windows when sonar was also detected (0.243), was 59% lower than the mean number detected in time windows when no sonar was detected (0.596). It took at least 3 hrs for GVP detection rates to return to the pre-exposure levels (Fig. 2). Time windows that included a sonar detection and which were within 3 hrs of each other were amalgamated into disturbance events. The average duration of these events was 6.6 hrs, although they ranged from 3 hrs to 34 hrs.

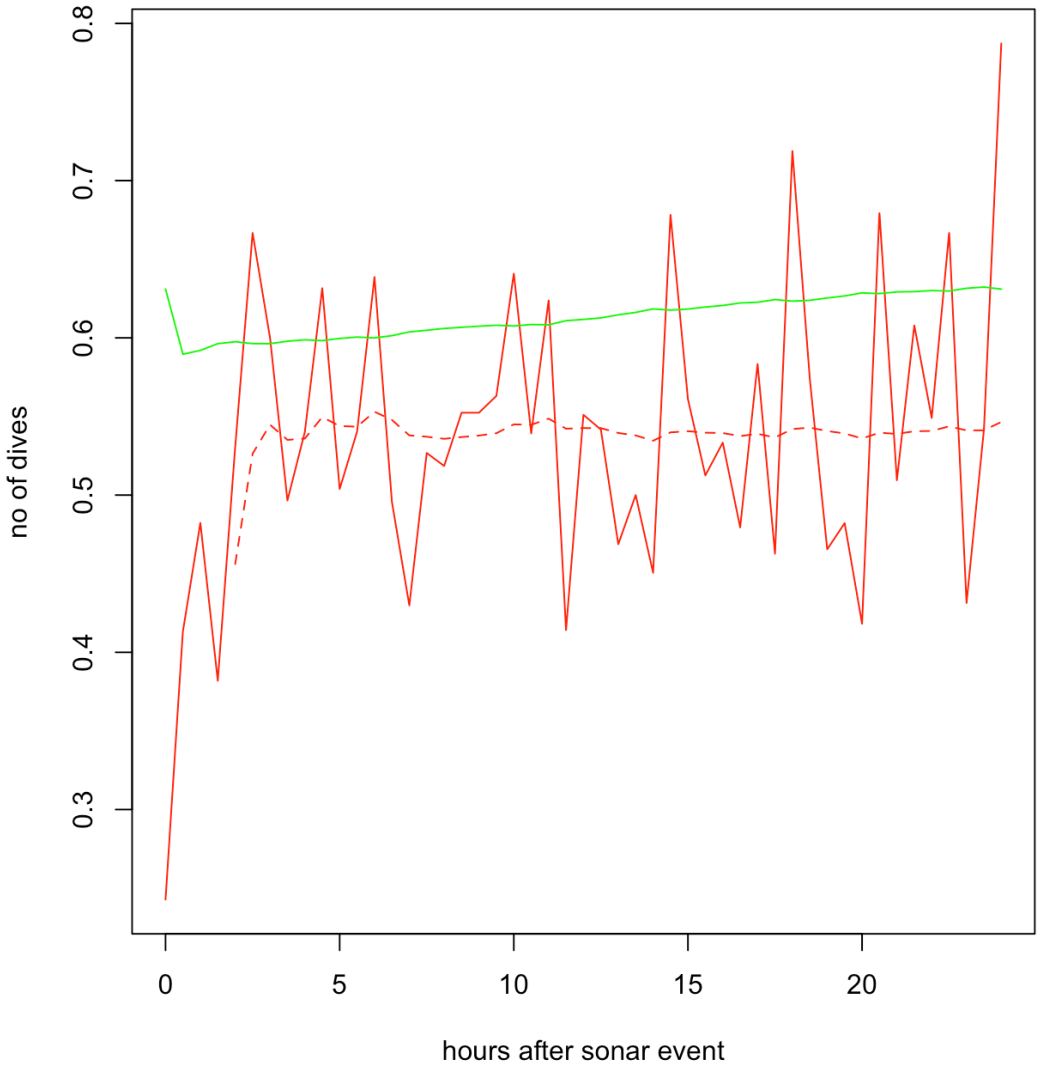

Figure 2. The mean number of Group Vocalization Periods (GVPs) detected on SOAR hydrophones within a 30 min time window. Solid red line = average number of GVPs detected in the 30 min window exactly X hrs after any sonar event. Dotted red line = average number of GVPs detected in all 30 min windows from 2 hrs after sonar event to X hrs. Solid green line = average number of GVPs detected in all 30 min windows that were not affected by sonar (i.e. the time windows that were not used to calculate the dotted red line at the same point)

Simulated disturbance histories were generated by assuming that the probability that an individual female was disturbed during a particular 30 min time window was 0.592 (1 - 0.243/0.596), and conducting a Binomial trial for each of the time windows in the 2015 archive when sonar was detected. We assumed that exactly the same pattern of sonar events occurred in all subsequent years. Disturbance was assumed to last for 6 time windows (i.e. 3 hrs) after each disturbance event, but the total period of disturbance on a particular day could be longer than this if an animal was predicted to be disturbed again exactly 3 hrs after the

initial disturbance. We assumed that the effect of disturbance on a particular day was to reduce energy intake by (total number of time windows disturbed)/48.

4. Results

Even large (i.e. old) simulated females were predicted to be unable to raise a calf successfully if they spent 100% of their time on SOAR (Fig. 3).

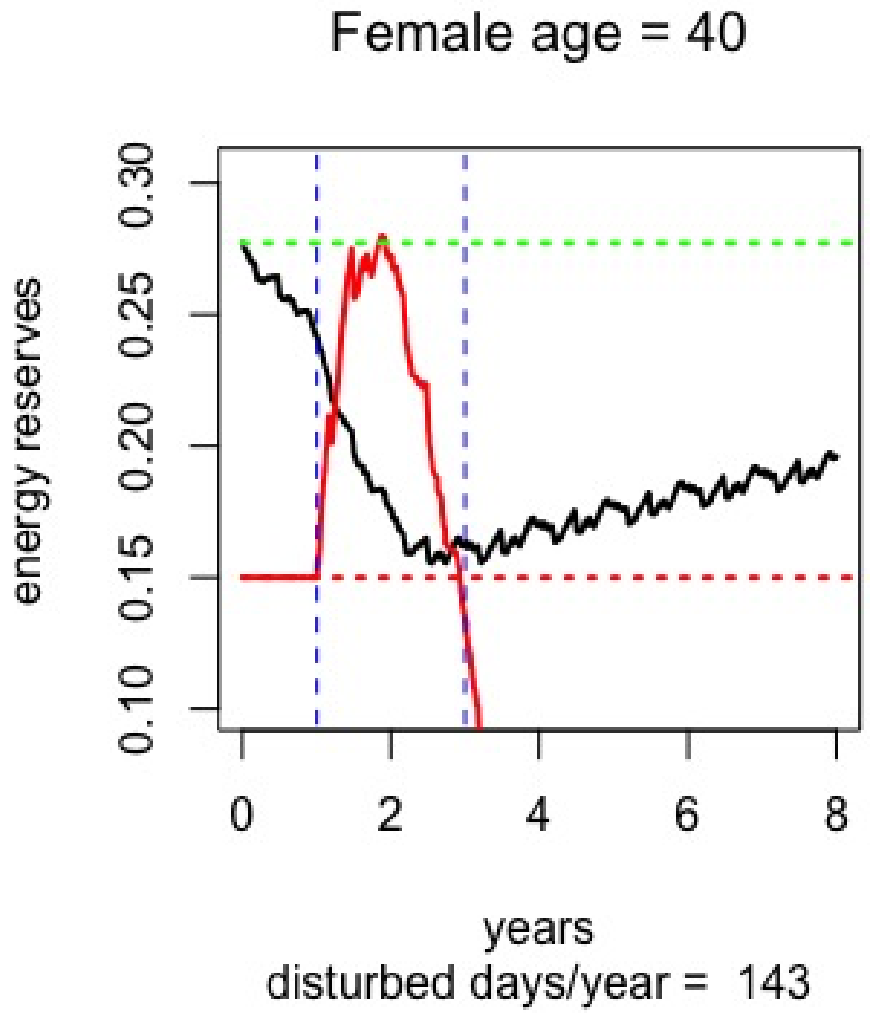

Figure 3. Predicted changes over time in the body condition of a 40 year-old female Zc and her calf over the course of pregnancy and lactation, assuming that the female spent 100% of her time on SOAR. Her calf is predicted to die mid-way through lactation. Notation as in Fig. 1.

Given the ratio of calves to adult females observed on SOAR (Falcone et al., this report), these predictions are clearly unrealistic. We therefore investigated the effects of disturbance if females spent only 50% of their time on SOAR. Fig. 4 indicates that older females are predicted to raise a calf successfully in these circumstances, but they take longer to recover to breeding condition after lactation than undisturbed females.

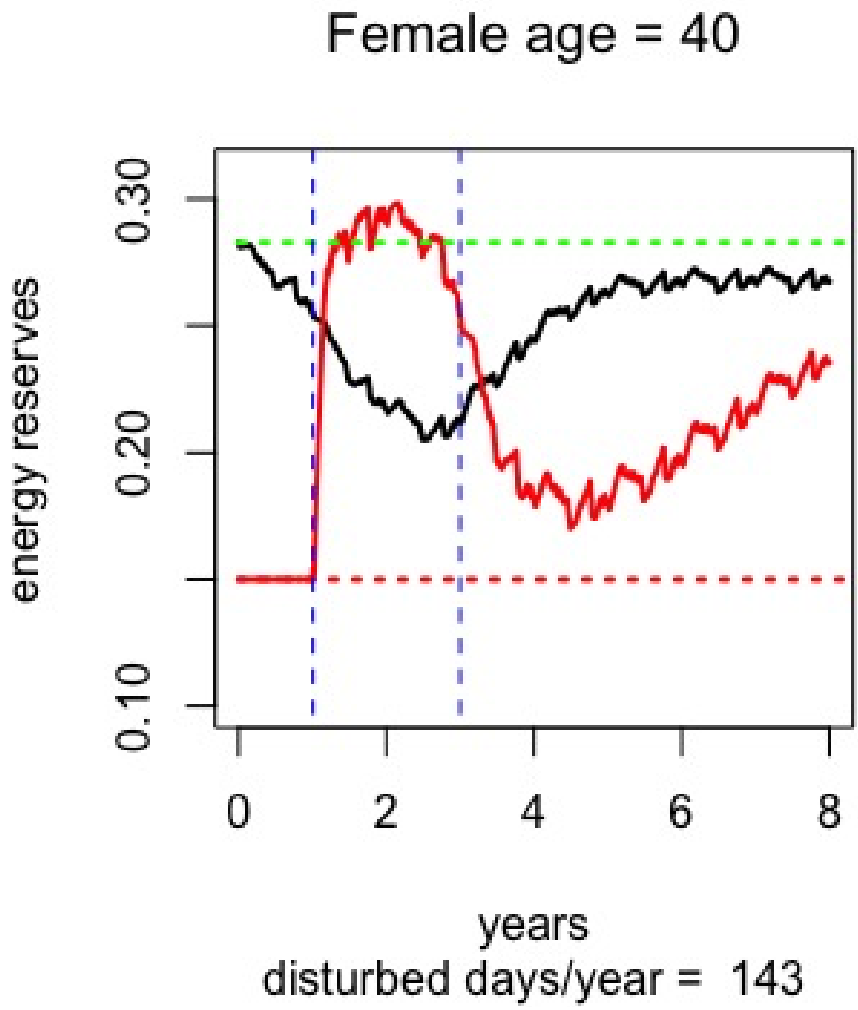

Figure 4. Predicted changes over time in the body condition of a 40 year-old female Zc and her calf over the course of pregnancy and lactation, assuming that the female spent 50% of her time on SOAR. Although she is able to raise her calf successfully, she may not be able to breed again for a number of years. Notation as in Fig. 1.

Falcone et al. (2017) suggested a more likely scenario: that there are "local ecological advantages that help to offset the presumed cost of inhabiting a busy military training range". We investigated this suggestion by increasing the value of *R* by 10% to simulate a more productive environment. In these circumstances, females as young as 12 years are predicted to breed successfully, even if they spend 100% of their time on SOAR (Fig. 5).

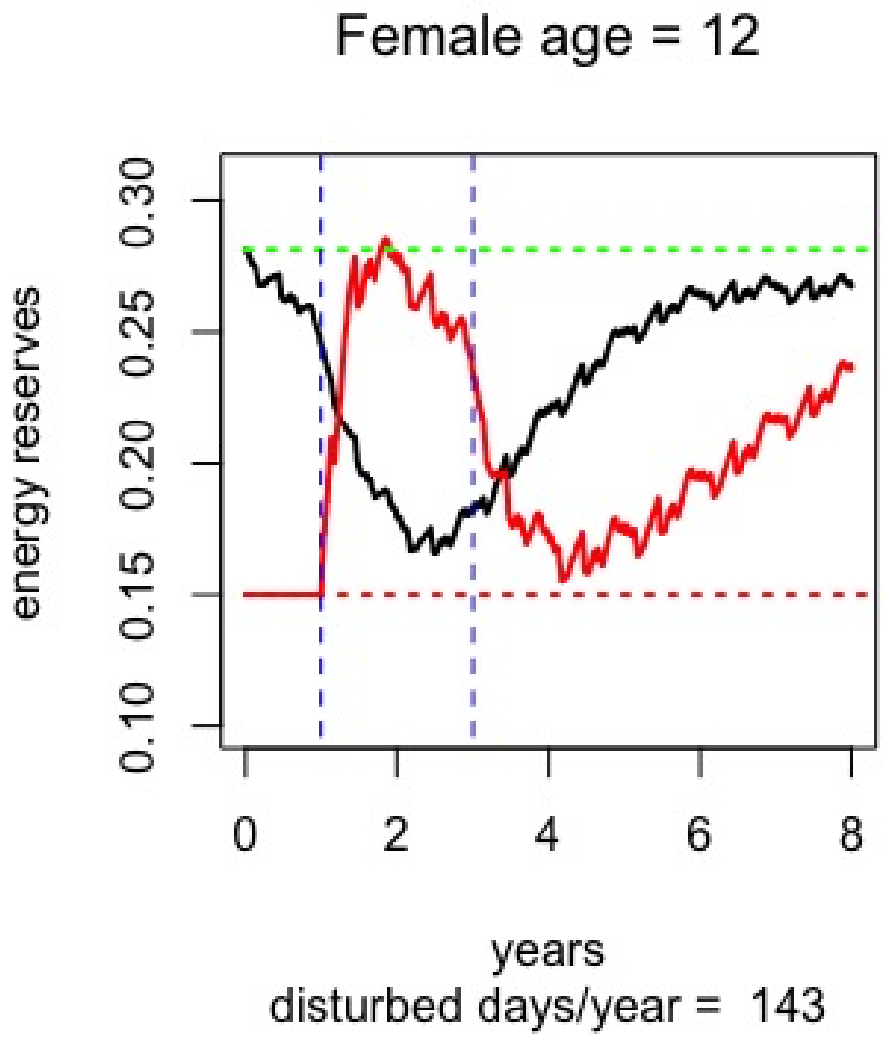

Figure 5. Predicted changes over time in the body condition of 12 year-old female Zc and her calf over the course of pregnancy and lactation, assuming that the female spent 100% of her time on SOAR. Environmental productivity was set 10% higher than in Figs. 1,3 & 4. Notation as in Fig. 1.

5. Discussion

The predictions of the life history consequences of disturbance from this preliminary bioenergetics model must be treated with great caution. Their use here is not to estimate the population-level effects of disturbance to *Zc* on SOAR but to illustrate the implications of different assumptions about the way in which disturbance may affect energy acquisition and the potential consequences of this for reproduction and survival. There are no estimates for the values of most of the parameters in the model, and a detailed sensitivity analysis is required to determine the robustness of the predictions to the values that were assumed for these parameters. We also need to incorporate the effects of fetal mortality, calf mortality that is not caused by starvation, ovulation rate and fertilization success into the bioenergetics model. All of these processes will affect predictions of the ratio of calves to adult females in the population. With these modifications it will be possible to generate predictions that can be compared with direct observations of tagged and individually-identified *Zc* on SOAR and at the proposed, undisturbed reference site off Guadalupe, Mexico.

6. Literature cited

Aoki, K., Sato, K., Isojunno, S., Narazaki, T., and Miller, P. J. O. 2017. High diving metabolic rate indicated by high-speed transit to depth in negatively buoyant long-finned pilot whales. *The Journal of Experimental Biology*, *220*(20), 3802–3811. http://doi.org/10.1242/jeb.158287

De Roos, A. M., N. Galic, and H. Heesterbeek. 2009. How resource competition shapes individual life history for nonplastic growth: ungulates in seasonal food environments. *Ecology*, *90*, 945–960.

Falcone, E. A., Schorr, G. S., Watwood, S. L., Deruiter, S. L., Zerbini, A. N., Andrews, R. D., … Moretti, D. J. (2017). Diving behaviour of Cuvier's beaked whales exposed to two types of military sonar. *Royal Society Open Science*, *4*, 170629. http://doi.org/10.1098/rsos.170629

Kooijman, S. A. L. M. 2010. Dynamic Energy Budget theory for metabolic organisation (Third edition.). Cambridge University Press, Cambridge, UK.

Lika, K., and S. A. L. M. Kooijman. 2011. The comparative topology of energy allocation in budget models. *Journal of Sea Research*, *66*, 381–391.

Lockyer, C. 1993. Seasonal Changes in Body Fat Condition of Northeast Atlantic Pilot Whales, and their Biological Significance. *Report of the International Whaling Commission, Special Issue 14,* 325–350.

Lockyer, C. 2007. All creatures great and smaller: a study in cetacean life history energetics. *Journal of the Marine Biological Association of the UK*, *87*, 1035–12.

Mead, J.G. 1984. Survey of Reproductive Data for the Beaked Whales (Ziphiidae). *Report of the International Whaling Commission, Special Issue 6*, 91-96.

Miller, C. A., D. Reeb, P. B. Best, A. R. Knowlton, M. W. Brown, and M. J. Moore. 2011. Blubber thickness in right whales *Eubalaena glacialis* and *Eubalaena australis* related with reproduction, life history status and prey abundance. *Marine Ecology Progress Series, 438*, 267–283.

New, L. F., D. J. Moretti, S. K. Hooker, D. P. Costa, and S. E. Simmons. 2013. Using Energetic Models to Investigate the Survival and Reproduction of Beaked Whales (Family Ziphiidae). *PLoS ONE, 8,* e68725–14. http://doi.org/10.1371/journal.pone.0068725.

Annex A

Modelling the Consequences of Seasonal Resource Fluctuations and Disturbance on the Life History of Female Long-Finned Pilot Whales (*Globicephala melas*)

Vincent Hin[a], John Harwood[b] & André M. de Roos[a]

[a] Institute for Biodiversity and Ecosystem Dynamics, University of Amsterdam, Amsterdam, The Netherlands; v.hin@uva.nl; A.M.deRoos@uva.nl
[b]Centre for Research into Ecological and Environmental Modelling, University of St Andrews, St Andrews, UK; jh17@st-andrews.ac.uk

Introduction

The increase of human activity in the marine environment has led to concern about the effects of disturbance on marine mammals (Halpern et al. 2008; DeRuiter et al. 2013; Maxwell et al. 2013; Fleishman et al. 2016; Parsons 2017). Several sources of disturbance (ship traffic, seismic surveys, use of military sonar) can lead to a variety of responses and impacts on marine mammals, such as decrease/cessation of feeding, avoidance behaviour, temporary and permanent effects on hearing, and death (National Research Council 2003). Especially the link between the use of military sonar and the stranding of whales and dolphins has received considerable attention (Cox et al. 2006; Parsons et al. 2008; Tyack et al. 2011; Parsons 2017).

While the link between disturbance and its (short term) effect on behaviour, feeding, and health of individuals is becoming more apparent (Miller 2012; Sivle et al. 2012; DeRuiter et al. 2013; Christiansen and Lusseau 2015; Friedlaender et al. 2016), assessing the (long-term) population consequences is still faced with many challenges and large uncertainties. These arise from (among others) the inaccessibility of the marine environment and the species in question, uncertainty about many life history parameters and processes, the difference in timescale between the disturbance event and the consequences for populations, and lack of information about behavioural responses that might aggravate or compensate the effect of a disturbance (Harwood and Stokes 2003; National Research Council 2005).

The PCoD (population consequences of disturbance) framework is a conceptual model to connect disturbance to its population-level consequences by means of a number of transfer functions (New et al. 2014; Harwood et al. 2016; Pirotta et al. 2018*a*). These transfer functions subsequently link the properties of disturbance to behavioural changes, life history functions, vital rates and population effects. Although the precise nature of many of these transfer functions is unknown, it is likely that they are highly context-dependent (National Research Council 2005; Friedlaender et al. 2016). For example, disturbance will have a different effect on lactating females in a resource-poor environment than on non-lactating females in a resource-rich environment. This context-dependency requires an approach that includes the state of the individual (e.g. energy reserve, reproductive status) and the state of the environment (e.g. resource density, presence of predators) to mediate between disturbance and biological significant changes in vital rates. Bio-energetic models represent such an approach and have been used to assess population consequences of disturbance for a variety a marine mammal species (New et al. 2013; Villegas-Amtmann et al. 2015; Costa et al. 2016; McHuron et al. 2016; Pirotta et al. 2018*b*). The downside, however, is the amount and quality of data needed to parameterize and validate these models, which are not available for many species (Harwood et al. 2016).

Bio-energetic models that assess the effect of disturbance on marine mammals focus on female life history and, in most cases, only take into account a single reproductive cycle (Braithwaite et al. 2015; Christiansen and Lusseau 2015; Villegas-Amtmann et al. 2015; McHuron et al. 2016; Pirotta et al. 2018*b*). From an energetics perspective, the reproductive period, and especially lactation, is the most demanding part of female life history and also of considerable importance for population growth. However, in order to assess under which conditions disturbance leads to negative population growth rates, it is necessary to model female life history and energetics across the entire life (Pirotta et al. n.d.). In absence of any density-dependence, population decline will occur when the expected lifetime reproductive output of a single female (R_0) is smaller than 1 (counting females only) (Caswell 2001). Accounting for males only becomes important in the presence of density-dependence, at least under the assumption that male density does not influence pregnancy rates of females. Therefore, it is possible to gain insight about the population consequences of disturbance in the absence of density-dependence by simply looking at the expected lifetime reproductive output of a single female.

Here we present a bio-energetics model of a single medium-sized cetacean to assess the population consequences of disturbance, depending on environmental context as quantified by resource availability. We model bio-energetics and life history across the entire life of a female individual. In addition, we follow calf survival and development until weaning. Although the structure of the model is general enough to describe the life history of any (marine) mammal species, we parameterize and tailor this model for long-finned pilot whales (*Globicephala melas*). The choice for this species is motivated by the relatively rich amount of data on pilot whale bio-energetics and life history processes (The International Whaling Commission 1993) and the observation that this species can be subject to (sound) disturbance (Wang and Yang 2006; Dolman et al. 2010; Miller 2012; Sivle et al. 2012; Wensveen et al. 2015; Isojunno et al. 2017). With this model, we aim to understand how disturbance affects reproductive abilities of the female and survival of the female and her calves, as integrated in the expected lifetime reproductive output of a single female. We assess the consequences of a yearly recurrent disturbance period that can vary in duration and the timing of onset within the year. The model assumes that individual pilot whale (both the female and her calves) can behaviourally compensate for disturbance by increasing feeding activity when body condition decreases and sufficient resources are available. We show how a number of life-history characteristics change with increasing disturbance intensity. Furthermore, we outline how the effects of disturbance depend on the productivity of the environment and its seasonal variation.

Model Formulation

The life history processes of the female and her calves (growth, reproduction and survival) depend on energy and a Dynamic Energy Budget (DEB) model specifies how assimilated energy is allocated between different processes (Lockyer 2007; Kooijman 2010; Lika and Kooijman 2011). Energy can temporarily be stored in a 'reserve compartment', which functions as a buffer between incoming and outgoing energy flows (De Roos et al. 2009). This reserve compartment models fat tissue that is mainly stored internally (in and around visceral organs and muscle tissue), but also in blubber of pilot whales (Lockyer 1993; 2007) and can be mobilized to serve energetic needs. The state of the reserve compartment is quantified by 'reserve density' and controls various life history functions (Lockyer 2007; Miller et al. 2011). Reserve density therefore links the effects of disturbance and environmental conditions to survival and reproduction and, ultimately population dynamics. To control for differences in

absolute size during ontogeny, we use relative reserve density (reserve mass over total body mass, also called body condition) as a measure of individual health. A good body condition is required for successful calf recruitment (pregnancy and lactation) and a poor body condition compromises survival and decreases life expectancy. The joint outcome of survival and reproduction is summarised as the expected lifetime reproductive output (R_0) of the female. More precisely, R_0 is defined as the expected number of weaned calves that a single female will produce from weaning age onwards. Maximum age at weaning, instead of age at birth, was chosen as a starting point for the calculation of R_0, because mammalian individuals only become independent from their mother at weaning. As a consequence, in the life history simulations the focal female is initiated at weaning. A description of the model's most important features is outlined below and summarised in Table 1. Full model details and parameters are presented in the Supplementary Material.

Bio-energetics

The DEB model that specifies the allocation of energy is taken from De Roos et al. (De Roos et al. 2009) and a schematic overview of the energy allocation scheme is shown in figure 1. Energy is derived from the environment through resource feeding and, in addition, calves derive energy from their mother through lactation. Energy is expended on field and maintenance metabolism, growth costs, gestation costs (when pregnant) and lactation costs (when lactating). The energy storage compartment ('energy reserves') is represented by reserve density (F in kg). All rates of energy flow (connecting lines in figure 1) depend on the state of the environment and the state of the individual. The environment state is captured by resource density (R), while the individual state consists of age (a, days), structural size (length l, cm. and mass S, in kg), reserve density (F, in kg) and reproductive status (see Table 1 for all individual state-variables and associated parameters). The structural component of an individual includes all tissue that cannot be used to fuel maintenance metabolism, lactation or gestation, such as bones and vital organs (Kooijman 2010). In contrast, assimilated energy or energy mobilized from the reserve compartment is used for such purposes. Structural mass changes due to structural growth. Dynamics of reserve density are given by the difference between total energy assimilation and total energy expenditure (see below).

Structural growth

Growth in structural mass of mammals is best represented by a demand type of growth, in which structural growth rate and asymptotic structural mass do not vary with the rate of assimilated energy. Instead, structural growth poses a certain energy demand on the environment. Based on pilot whale data in (Bloch et al. 1993), we use a Von Bertalanffy length-age relationship $l(a)$ for free-living individuals with the length at birth $l_b = 177$, asymptotic length $l_\infty = 450$ and Von Bertalanffy growth rate $k = 0.00045$ (Table 1). The length-age relationship of a foetus ($l_p(\tau_p)$) is a linear function of time since conception, τ_p, such that foetuses reach length at birth (l_b) when the gestation period (T_P) is due. Length is converted to structural mass (S) by a power function (Bloch et al. 1993). Total body weight, W, equals the sum of structural mass S and reserve density F. For pregnant females, W also includes the structural mass of the foetus $S(l_p(\tau_p))$. Body condition, or relative reserve density is defined as F/W.

Resource feeding

Resource assimilation rate scales with structural surface-area ($S^{2/3}$, (Kooijman 2010)) and increases linearly with resource density R. The assumption of a linear functional response is based on the proposition that resource handling time and/or digestion rarely limits resource intake rate in long-finned pilot whales. This assumption seems appropriate for species that dive to find their food and spend most of their time at the surface (Baird et al. 2002; Heide-Jorgensen et al. 2002; Isojunno et al. 2017). Resource density is measured in assimilated energy per unit volume ($\mathrm{MJ} \cdot \mathrm{m}^{-3}$) and therefore includes assimilation and conversion efficiencies of prey items by pilot whale individuals. The resource ingestion rate is furthermore proportional to resource feeding level, which operates as a negative feedback of body condition on resource intake to ensure that the reserve density does not grow out of bounds under favourable conditions (high resource availability or low energy expenditure). Similarly, the increase in feeding level when body condition is low can be seen as a behavioural compensation response to disturbance or low resource availability. The feeding level (0 – 1) is implemented as a decreasing sigmoidal function of body condition that equals 0.5 at the target body condition (parameter ρ). (Lockyer 1993) notes that body condition of pilot whales is independent of age and reproductive status and finds no evidence for an energy storage strategy to fulfil energetic demands of reproduction. Consequently, we use a constant target body condition of 0.30 (Supplementary Material). Finally, independent resource feeding depends on age in order to simulate the observation that young individuals are inexperienced resource foragers and that foraging skills increase with age (Lockyer 2007; Isojunno et al. 2017).

Milk consumption

In addition to resource feeding, calves gain energy through milk consumption with rate: $I_L(a, S, F, W, F_m, W_m)$. Like resource feeding, milk consumption scales with a two-thirds power of structural mass ($S^{2/3}$), and is furthermore proportional to the lactation scalar ϕ_L. Milk suckling decreases with increasing body condition of the calf in the same way as resource intake decreases with body condition. The mother also regulates milk provisioning, in a manner that depends on her own body condition ($^{F_m}/_{W_m}$). When the mother's body condition declines, milk provisioning is decreased and when her body condition reached the starvation threshold ρ_s, the mother ceases milk supply altogether. Finally, milk consumption depends on calf age. Beyond the first year of lactation, milk consumption decreases such that it becomes zero at the age of weaning, T_L. At T_L the calf becomes independent of the focal female and is no longer tracked during simulation. At any time before T_L the milk supply will be interrupted or terminated only if the mother's body condition falls below ρ_s. The possibility of early weaning resulting from good body condition of mother and calf is not modelled. However, due to the feedbacks of milk supply with female and calf body condition, milk consumption will be limited under these circumstances. Based on data in (Martin and Rothery 1993) we adopt $T_L = 1223$. The parameters ϕ_L and ρ_s were derived to be 2.7 and 0.15, respectively (see Supplementary Material).

Energetic costs

Energetic costs are comprised of: $C_M(W_M)$; field metabolic costs depending on the maintenance body weight (W_M), $C_G(S)$; costs of growth in structural size, $C_P(\tau_p)$; pregnancy costs depending upon time since fertilization and $C_L(F, W, a_c, S_c, F_c, W_c)$; lactation costs depending upon both age and body condition of the calf (subscript c indicates a calf variable), in addition to the body condition of the mother. Field metabolic costs are composed of the

metabolic costs of maintenance and daily routine activity. Since maintenance of one kg. of reserve density is lower than that of one kg of structure, we introduce the maintenance body weight W_M. This measure uses the proportionality constant θ_F to discount the contribution of reserve density to maintenance costs (see Table 1), which was set to 0.2. Field metabolic costs are a σ_M-multiple of the maintenance weight, raised to the ¾ power following (Kleiber 1975). Somatic growth costs are equal to the derivative of the Von Bertalanffy growth function in structural mass, with proportionality constant σ_G. The same holds for pregnancy costs, which are equal to the derivative of the foetal growth in structure times σ_G. Lactation costs equal the milk provisioning rate I_L, corrected by a conversion factor $\sigma_L = 0.86$ that accounts for efficiency of milk production (by the mother) and milk assimilation (by the calf) based on data from (Lockyer 1993).

Reserve dynamics

Dynamics of reserves density follow from adding and subtracting anabolic and catabolic processes and accounting for the conversion efficiency of catabolism and anabolism. Independent of individual status, reserve density increases due to resource assimilation and decrease with field metabolic costs and somatic growth costs. For calves, milk suckling, in addition to resource feeding, increases reserve density. For pregnant and lactating females, reserve density further decreases through gestation and lactation costs, respectively. The conversion efficiency (ε_i) equals ε^+ if reserve dynamics are anabolic ($dF/da > 0$) and ε^- if reserve dynamics are catabolic ($dF/da < 0$). Reserve dynamics are:

$$\frac{dF}{da} = \begin{cases} \varepsilon_i^{-1}(I_R(a,R,S,F,W) + I_L(a,S,F,W,F_m,W_m) - C_G(l) - C_M(W_M)) & \text{Calves} \\ \varepsilon_i^{-1}(I_R(a,R,S,F,W) - C_G(l) - C_M(W_M) - C_P(\tau_c)) & \text{Gestating fem} \\ \varepsilon_i^{-1}(I_R(a,R,S,F,W) - C_G(l) - C_M(W_M) - C_L(F,W,a_c,S_c,F_c,W_c)) & \text{Lactating fema} \\ \varepsilon_i^{-1}(I_R(a,R,S,F,W) - C_G(l) - C_M(W_M)) & \text{Otherwise} \end{cases} \quad (3)$$

Survival and life expectancy

In order to calculate lifetime reproductive output, we track survival probabilities of A focal female and her calves. There are two sources of mortality that decrease survival probability: age-dependent mortality and starvation-induced mortality. Age-dependent mortality applies to all individuals and consists of *i*): juvenile mortality that decreases with age, *ii*): senescence mortality that increases with age and *iii*): background mortality that is constant with age (Barlow and Boveng 1991; Bloch et al. 1993). Starvation-induced mortality is only applied when the body condition of an individual falls below the starvation threshold (ρ_s). Starvation mortality increases with declining body condition according to a hyperbolic function, with the speed of increase controlled by parameter μ_s (De Roos et al. 2009).

Depending on the purpose of the simulation, life expectancy is either fixed or determined randomly. A fixed life expectancy is used when illustrating the consequences of disturbance across the entire life of the focal female. In this case, the maximum female life expectancy of 60 years is used (Bloch et al. 1993; Lockyer 2007). When applying the age-dependent mortality as described above, this corresponds to a survival threshold of $2.266 \cdot 10^{-7}$. Therefore, the female is considered dead when her survival falls below this threshold, which in absence of starvation mortality happens at an age of 60 years. However, when survival is also decreased by starvation mortality, the female's life expectancy is decreased since she

will cross the survival threshold at a younger age. The fixed life expectancy of 60 years is also used for the calves and implies that calves only die if their survival falls below $2.266 \cdot 10^{-7}$ before they reach weaning age. Obviously, this will only happen with a substantial amount of starvation mortality.

A randomly determined life expectancy is used when calculating the expected lifetime reproductive output (R_0) of the focal female. The calculation of R_0 requires using the mean life expectancy of a female, in contrast to the maximum life expectancy of 60 years. Besides this, the random event of a calf death introduces variation in the timing of the next reproduction, essentially creating an infinite number of possible life histories for the female. An accurate estimate of R_0 requires averaging the reproductive output over all those possible life histories, or at least of a substantial subset. The randomly determined life expectancy is implemented by assigning a random number between zero and one to the female at weaning age and to each calf at birth. The individual is considered death when the survival probability falls below this threshold value. Both R_0 and mean life expectancy can then be calculated by averaging the reproductive output and age at death of a sufficiently large number of life history simulations. For both random and fixed life expectancies, an individual also dies when its relative reserve density drops below 0.005.

Reproduction

At any time, the female will be in one of the following reproductive classes: resting, receptive, pregnant, lactating, and both receptive and lactating. A non-pregnant and non-lactating female will either be resting or receptive and this is determined by whether the absolute amount of reserves is above or below the pregnancy threshold. This threshold is equal to the reserve density required to produce a neonate ($F_{neonate}$), on top of the reserve density needed to offset starvation ($\rho_s W$). Here, the quantity $F_{neonate}$ is composed of *i)* the cost of producing the structural mass of a neonate from reserves of the mother and *ii*) the amount of reserves transferred at birth from the mother to the neonate. Foetuses are assumed to grow in structural mass only and at birth they receive an amount of reserves that equals the starvation level threshold for neonates ($\rho_s W_b$).

A non-pregnant and non-lactating female is assigned to the 'resting' state if her reserve density is below the pregnancy threshold. When the reserve level of the female crosses the threshold (*i.e.* $F > \rho_s W + F_{neonate}$) she becomes receptive and awaits implantation, as she does not become pregnant immediately. The receptive period (T_D) lasts for an average of 445 days, which is determined by the ovulation rate (assuming one ovulation per year) and the chance of successful insemination (0.82 see Supplementary Material). Pregnancy starts when the receptive period is due, irrespective of the reserve density at that point in time. Pregnancy lasts for $T_P = 365$ days. Lactation is initiated after the birth of the calf and lasts $T_L = 1223$ days, unless the calf dies, or the mother stops milk provisioning due to poor body condition. When a female is within the final T_P days of lactation, she can become receptive again if her reserve density is above the pregnancy threshold. This additional condition prevents the occurrence of two calves that simultaneously feed from the mother. In principle, the female could also be pregnant and lactating simultaneously, although the fact that the receptive period is longer than the gestation period ($T_D > T_P$) prevents this from happening. The shortest possible interval between a weaning event and the next onset of pregnancy is hence $445 - 364 = 81$ days and the shortest possible inter-birth and inter-weaning interval is 4.57 years ($81 + 365 + 1223$ days).

Resource dynamics and disturbance

Environmental resource density R fluctuates around a yearly mean value $\bar{R}$ with a seasonal pattern (period is 365 days) and a relative amplitude of A (0 – 1):

$$R = \bar{R}\left(1.0 - A\cos\left(\frac{2\pi(t + 91.25)}{365}\right)\right)$$

With seasonal variation ($A > 0$), resource density is at its mean value $\bar{R}$ and increasing on the first day of each year (t = 0, 365, etc.), which we arbitrary label as the middle of spring. Since the simulation starts at t = 0, the simulated life of the focal female is therefore initiated in the middle of spring. With seasonal variation, the resource density peaks at t = 91 days, which we call the middle of summer, and reaches its minimum in the middle of winter, at t = 273 days. Disturbance is modelled by a yearly recurrent cessation of feeding for a certain number of days per year. Consequently, disturbance is characterized by a disturbance period (number of days) and a starting date. Concerning the latter, we distinguish between summer (starting at $(t \bmod 365) = 91$ days) and winter disturbance (starting at $(t \bmod 365) = 273$). During the disturbance period the resource ingestion rates of the calf and the female are set to zero. Lactation is still possible during disturbance.

References

Alerstam, T., A. Hedenstrom, and S. Akesson. 2003. Long-distance migration: evolution and determinants. Oikos 103:247–260.

Baird, R. W., J. F. Borsani, M. B. Hanson, and P. L. Tyack. 2002. Diving and night-time behavior of long-finned pilot whales in the Ligurian Sea. Marine Ecology Progress Series 237:301–305.

Barlow, J., and P. Boveng. 1991. Modeling Age-Specific Mortality for Marine Mammal Populations. Marine Mammal Science 7:50–65.

Bloch, D., C. Lockyer, and M. Zachariassen. 1993. Age and Growth Parameters of the Long-Finned Pilot Whale off the Faroe Islands. Biology of Northern Hemisphere Pilot Whales 163–207.

Braithwaite, J. E., J. J. Meeuwig, and M. R. Hipsey. 2015. Optimal migration energetics of humpback whales and the implications of disturbance. Conservation Physiology 3:cov001–15.

Caswell, H. 2001. Construction, analysis, and interpretation. Sunderland: Sinauer.

Christiansen, F., and D. Lusseau. 2015. Linking Behavior to Vital Rates to Measure the Effects of Non-Lethal Disturbance on Wildlife. Conservation Letters 8:424–431.

Costa, D. P., L. Schwarz, P. Robinson, R. S. Schick, P. A. Morris, R. Condit, D. E. Crocker, et al. 2016. A Bioenergetics Approach to Understanding the Population Consequences of Disturbance: Elephant Seals as a Model System. Pages 161–169 *in* A. N. Popper and A. Hawkins, eds. The Effects of Noise on Aquatic Life II, Advances in Experimental Medicine and Biology (Vol. 875). Springer New York, New York, NY.

Cox, T. M., T. J. Ragen, A. J. Read, E. Vos, R. W. Baird, K. Balcomb, J. Barlow, et al. 2006. Understanding the impacts of anthropogenic sound on beaked whales 7:177–187.

De Roos, A. M., N. Galic, and H. Heesterbeek. 2009. How resource competition shapes individual life history for nonplastic growth: ungulates in seasonal food environments. Ecology 90:945–960.

DeRuiter, S. L., B. L. Southall, J. Calambokidis, W. M. X. Zimmer, D. Sadykova, E. A. Falcone, A. S. Friedlaender, et al. 2013. First direct measurements of behavioural responses by Cuvier's beaked whales to mid-frequency active sonar. Biology Letters

9:20130223–20130223.
Desportes, G., and R. Mouritsen. 1993. Preliminary Results on the Diet of Long-Finned Pilot Whales off the Faroe Islands. Report of the International Whaling Commission, Special Issue 14:305–324.
Dolman, S. J., E. Pinn, R. J. Reid, J. P. Barley, R. Deaville, P. D. Jepson, M. OConnell, et al. 2010. A note on the unprecedented strandings of 56 deep-diving whales along the UK and Irish coast. Marine Biodiversity Records 1–11.
Fleishman, E., D. P. Costa, J. Harwood, S. Kraus, D. Moretti, L. F. New, R. S. Schick, et al. 2016. Monitoring population-level responses of marine mammals to human activities. Marine Mammal Science 32:1004–1021.
Friedlaender, A. S., E. L. Hazen, J. A. Goldbogen, A. K. Stimpert, J. Calambokidis, and B. L. Southall. 2016. Prey-mediated behavioral responses of feeding blue whales in controlled sound exposure experiments. Ecological Applications 26:1075–1085.
Halpern, B. S., S. Walbridge, K. A. Selkoe, C. V. Kappel, F. Micheli, C. D'Agrosa, J. F. Bruno, et al. 2008. A Global Map of Human Impact on Marine Ecosystems. Science 319:948–952.
Harwood, J., and K. Stokes. 2003. Coping with uncertainty in ecological advice: lessons from fisheries. Trends in Ecology & Evolution 18:617–622.
Harwood, J., S. King, C. Booth, C. Donovan, R. S. Schick, L. Thomas, and L. New. 2016. Understanding the Population Consequences of Acoustic Disturbance for Marine Mammals. Pages 417–423 *in* A. N. Popper and A. Hawkins, eds. The Effects of Noise on Aquatic Life II, Advances in Experimental Medicine and Biology (Vol. 875). Springer New York, New York, NY.
Heide-Jorgensen, M. P., D. Bloch, E. Stefansson, B. Mikkelsen, L. H. Ofstad, and R. Dietz. 2002. Diving behaviour of long-finned pilot whales *Globicephala melas* around the Faroe Islands. Wildlife Biology 8:307–313.
Isojunno, S., D. Sadykova, S. DeRuiter, C. Curé, F. Visser, L. Thomas, P. J. O. Miller, et al. 2017. Individual, ecological, and anthropogenic influences on activity budgets of long-finned pilot whales. Ecosphere 8:e02044–26.
Kleiber, M. 1975. The fire of life: an introduction to animal energetics. R.E. Krieger Pub. Co., Huntington, N.Y.
Kooijman, S. A. L. M. 2010. Dynamic Energy Budget theory for metabolic organisation (Third edition.). Cambridge University Press, Cambridge, UK.
Lika, K., and S. A. L. M. Kooijman. 2011. The comparative topology of energy allocation in budget models. Journal of Sea Research 66:381–391.
Lockyer, C. 1993. Seasonal Changes in Body Fat Condition of Northeast Atlantic Pilot Whales, and their Biological Significance. Biology of Northern Hemisphere Pilot Whales 325–350.
Lockyer, C. 2007. All creatures great and smaller: a study in cetacean life history energetics. Journal of the Marine Biological Association of the UK 87:1035–12.
Martin, A. R., and P. Rothery. 1993. Reproductive Parameters of Female Long-Finned Pilot Whales (*Globicephala melas*) Around the Faroe Islands. Biology of Northern Hemisphere Pilot Whales 263–304.
Maxwell, S. M., E. L. Hazen, S. J. Bograd, B. S. Halpern, G. A. Breed, B. Nickel, N. M. Teutschel, et al. 2013. Cumulative human impacts on marine predators. Nature Communications 4:2688.
McHuron, E. A., D. P. Costa, L. Schwarz, and M. Mangel. 2016. State-dependent behavioural theory for assessing the fitness consequences of anthropogenic disturbance on capital and income breeders. (J. Matthiopoulos, ed.)Methods in Ecology and Evolution 8:552–560.

Miller, C. A., D. Reeb, P. B. Best, A. R. Knowlton, M. W. Brown, and M. J. Moore. 2011. Blubber thickness in right whales Eubalaena glacialis and Eubalaena australis related with reproduction, life history status and prey abundance. Marine Ecology Progress Series 438:267–283.
Miller, P. 2012. The Severity of Behavioral Changes Observed During Experimental Exposures of Killer (Orcinus orca), Long-Finned Pilot (Globicephala melas), and Sperm (Physeter macrocephalus) Whales to Naval Sonar. Aquatic Mammals 38:362–401.
National Research Council. 2003. *Ocean Noise and Marine Mammals*. The National Academies Press, Washington, DC.
National Research Council. 2005. *Marine Mammal Populations and Ocean Noise*. National Academies Press, Washington, DC.
New, L. F., D. J. Moretti, S. K. Hooker, D. P. Costa, and S. E. Simmons. 2013. Using Energetic Models to Investigate the Survival and Reproduction of Beaked Whales (family Ziphiidae). (Y. Ropert-Coudert, ed.)PLoS ONE 8:e68725–14.
New, L. F., J. S. Clark, D. P. Costa, E. Fleishman, M. A. Hindell, T. Klanjšček, D. Lusseau, et al. 2014. Using short-term measures of behaviour to estimate long-term fitness of southern elephant seals. Marine Ecology Progress Series 496:99–108.
Parsons, E. C. M. 2017. Impacts of Navy Sonar on Whales and Dolphins: Now beyond a Smoking Gun? Frontiers in Marine Science 4:78–11.
Parsons, E. C. M., S. J. Dolman, A. J. Wright, N. A. Rose, and W. C. G. Burns. 2008. Navy sonar and cetaceans: Just how much does the gun need to smoke before we act? Marine Pollution Bulletin 56:1248–1257.
Pirotta, E., C. G. Booth, D. P. Costa, E. Fleishman, S. Kraus, D. Lusseau, D. Moretti, et al. 2018*a*. Understanding the population consequences of disturbance. Ecology and Evolution 1–13.
Pirotta, E., M. Mangel, D. P. Costa, B. Mate, J. A. Goldbogen, D. M. Palacios, L. A. Hückstädt, et al. 2018*b*. A Dynamic State Model of Migratory Behavior and Physiology to Assess the Consequences of Environmental Variation and Anthropogenic Disturbance on Marine Vertebrates. The American Naturalist 191:E40–E56.
Pirotta, E., M. Mangel, D. P. Costa, J. Goldbogen, J. Harwood, V. Hin, L. M. Irvine, et al. n.d. Anthropogenic disturbance in a changing environment: modelling lifetime reproductive success to predict the consequences of multiple stressors on a migratory population.
Sivle, L. D., P. H. Kvadsheim, A. Fahlman, F.-P. Lam, P. Tyack, and P. Miller. 2012. Changes in dive behavior during naval sonar exposure in killer whales, long-finned pilot whales, and sperm whales. Frontiers in Physiology 3.
Stearns, S. C. 1992. The Evolution of Life Histories. OUP Oxford.
Stephens, P. A., A. I. Houston, K. C. Harding, I. L. Boyd, and J. M. McNamara. 2014. Capital and income breeding: the role of food supply. Ecology 95:882–896.
The International Whaling Commission. 1993. *Biology of Northern Hemisphere Pilot Whales*. (G. P. Donovan, C. H. Lockyer, & A. R. Martin, eds.).
Tyack, P. L., W. M. X. Zimmer, D. Moretti, B. L. Southall, D. E. Claridge, J. W. Durban, C. W. Clark, et al. 2011. Beaked Whales Respond to Simulated and Actual Navy Sonar. (S. Thrush, ed.)PLoS ONE 6:e17009–15.
Villegas-Amtmann, S., L. K. Schwarz, J. L. Sumich, and D. P. Costa. 2015. A bioenergetics model to evaluate demographic consequences of disturbance in marine mammals applied to gray whales. Ecosphere 6:art183–19.
Wang, J. Y., and S.-C. Yang. 2006. Unusual cetacean stranding event of Taiwan in 2004 and 2005. J. Cetacean Res. Manage. 8:283–292.
Wensveen, P. J., A. M. von Benda-Beckmann, M. A. Ainslie, F.-P. A. Lam, P. H.

Kvadsheim, P. L. Tyack, and P. J. O. Miller. 2015. How effectively do horizontal and vertical response strategies of long-finned pilot whales reduce sound exposure from naval sonar? Marine Environmental Research 106:68–81.

Table 1: Overview of the most important model variables and parameters.

Variable, parameter	Unit	Description	Value
Resource			
$\bar{R}$	MJ·m^{-3}	Mean resource density in assimilated energy units	1.6 – 3.0
A	–	Relative amplitude of seasonal resource variation	0, 0.15, 0.3, 0.45
Age			
a	days	Individual age	–
τ_p	days	Time since conception	–
T_P	days	Gestation time	365
T_L	days	Lactation time	1223
T_D	days	Receptive period	445
Reserves			
F	kg	Reserve density	–
–	kg	Pregnancy threshold	$F > \rho_s W + F_{neonate}$
$F_{neonate}$	kg	Amount of reserves to create a newborn individual	61.45
$F/_W$	–	Body condition	–
ρ	–	Target body condition	0.3
ρ_s	–	Starvation threshold	0.15
Length			
$l(a)$	cm	Length-age relationship free-living individual	$l_\infty - (l_\infty - l_b)e^{-ka}$
l_b	cm	Length at birth	177
l_∞	cm	Asymptotic length	450
k	day^{-1}	Von Bertalanffy growth rate	0.00045
$l_p(\tau_p)$	cm	Length-age relationship foetus	$l_b \frac{\tau_p}{T_P}$
Structural mass			
$S(l)$	kg	Structural mass-length relationship	$\omega_1 l(a)^{\omega_2}$
ω_1	kg·cm$^{-\omega_2}$	Mass-length scaling constant	8.5·10^{-5}

ω_2	–	Mass-length scaling exponent	2.6
Body weight			
$W(S,F,\tau_p)$	kg	Total body mass	$\begin{cases} S+F+S\left(l_p(\tau_p)\right) & \text{pregnant} \\ S+F & \text{otherwise} \end{cases}$
$W_M(S,F,\tau_p)$	kg	Maintenance body mass	$\begin{cases} S+\theta_F F+S\left(l_p(\tau_p)\right) & \text{pregnant} \\ S+\theta_F F & \text{otherwise} \end{cases}$
θ_F	–	Relative maintenance costs of reserves	0.2

Table 2: Modelled energetics of an undisturbed, fully-grown female with structural mass 672 kg living in a non-seasonal environment with $\bar{R} = 1.8$ and other parameters as default (Table S2). Mean (min – max) values represent rates in MJ · day^{-1}. Totals (in MJ) are integrated over the whole period.

	Mean	% increased	Total
Reserve density			
At equilibrium	260	0 (reference value)	
During recovery	245 (233 – 254)	-5.7% (-10 – -2.3)	
During pregnancy	257 (253 – 258)	-1.2% (-2.7 – -0.8)	
During lactation	217 (213 – 248)	-16% (-18 – -4.6)	
Resource assimilation			
For metabolism	103	0 (reference value)	
Recovering	118 (111 – 126)	15% (7.8 – 22)	
Pregnant	112 (106 – 123)	8.7% (2.9 – 19)	
Lactating	133 (116 – 134)	29% (13 – 30)	
Pregnancy costs			
Structural growth foetus	4.9 (0 – 13)		1787
Metabolic rate during pregnancy	106 (104 – 111)	2.9% (1.0 – 7.7)	
Lactation costs			
First year	31 (29 – 44)		11476
Whole period	30 (0.2 – 44)		36210
Calf milk assimilation			
First year	27 (25 – 38)		9870
Whole period	25 (0.2 – 38)		31140
Calf resource assimilation			
First year	2.7 (0 – 7.1)		1017
Whole period	13 (0 – 42)		16338

Figure 1: Schematic overview of the Dynamic Energy Budget model that controls pilot whale life history. Boxes indicate different sources (green) and destinations (red) of energy flows (connecting lines). Incoming and outgoing energy flows are denoted by I_i and C_i, respectively. I_T and C_T represent total incoming and outgoing energy flow, the difference of which constitutes the reserve dynamics (blue). Solid lines represent energy flows for all individuals, while dashed lines are energy flows that dependent on individual state. Reprinted from (De Roos et al. 2009)

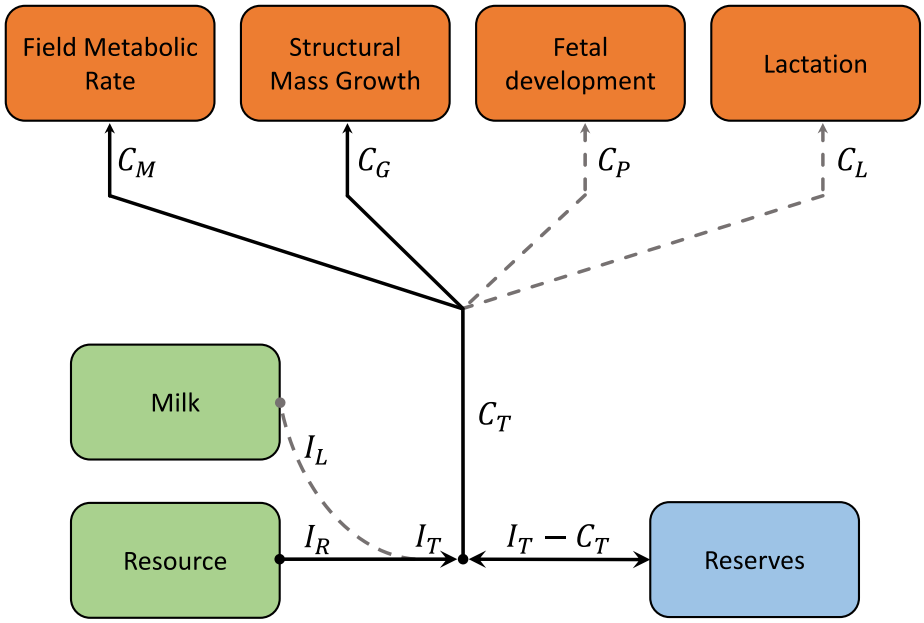

Figure 2: Reserve density of the female and her calves as a function of female age for different disturbance periods (0, 15 & 25 days per year). Female reserve density is coloured according to reproductive status (as indicated). A non-pregnant and non-lactating female is coined 'receptive' when her reserve density is above the pregnancy threshold (not shown) and she awaits implantation, otherwise she is coined 'resting'. Target reserve densities (grey lines) are equal to $\rho = 0.3$ times total body weight, while starvation thresholds (black lines) are $\rho_s = 0.15$ times total body weight. Life history statistics in each plot: LRO = lifetime reproductive output (counting female offspring only), AfR = age at first reproduction (yrs), LE = life expectancy (yrs), IBI = inter-birth interval (yrs) and IWI = inter-weaning interval (yrs). These life histories are created by using a fixed life expectancy of 60.3 years that only decreases with starvation mortality. Mean annual resource density $\bar{R} = 1.8$, all other parameters at default values (Table S2).

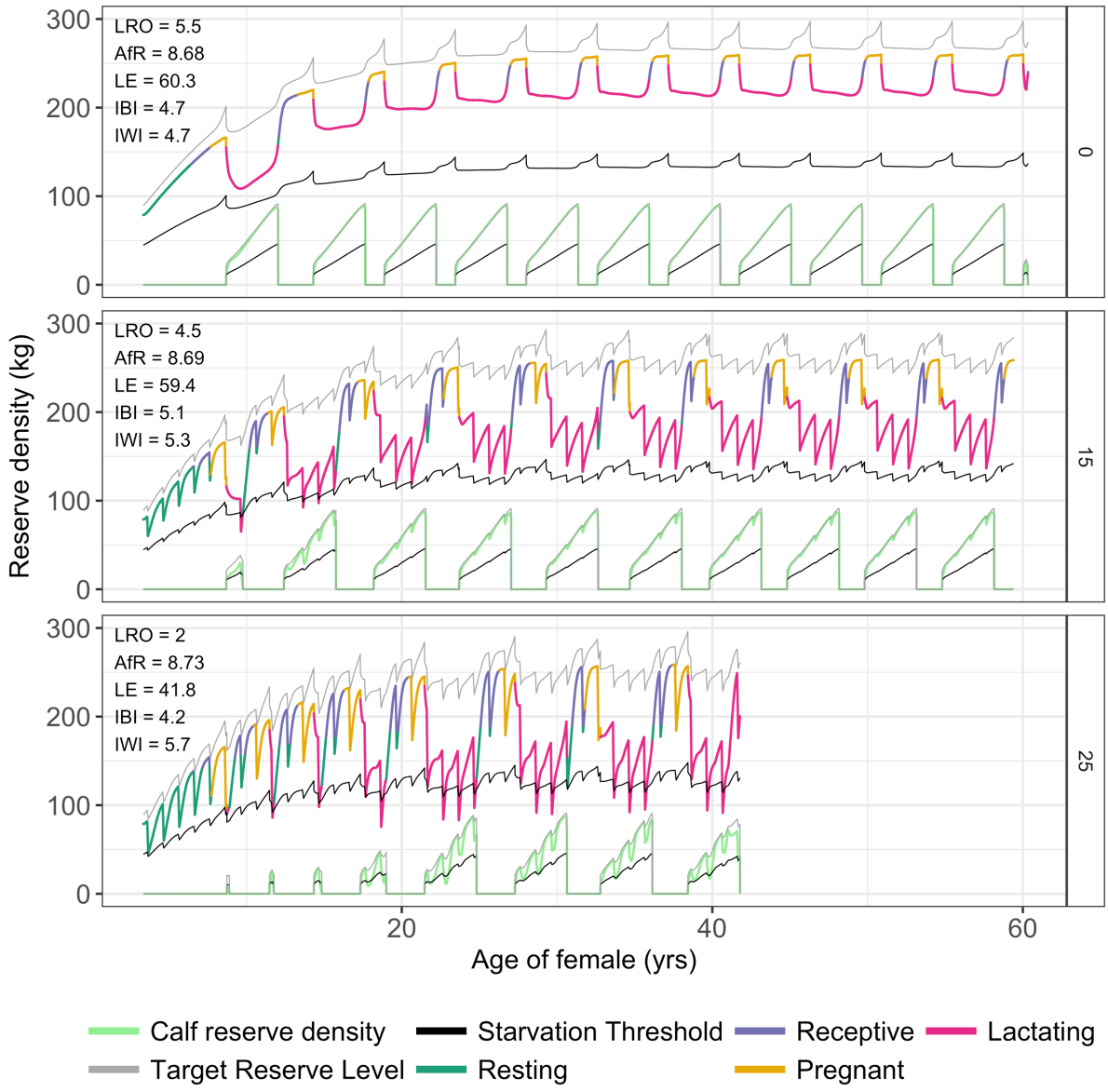

SUPPLEMENTARY MATERIAL

of

Modelling the Consequences of Seasonal Resource Fluctuations and Disturbance on the Life History of Female Long-Finned Pilot Whales (*Globicephala melas*)

Vincent Hin, John Harwood & André M. de Roos

Model Description

All model equations are summarised in table S1, while the most important model features are listed in table 1 of the main text. The two individual-state (*i*-state) variables are age (a in days) and reserve density (F in kg.). We also track the structural length (l in cm), structural mass (S in kg.), total body weight (W in kg) and maintenance body weight W_M of each individual, but these quantities are all functions of age and/or reserve density. For the female, we track whether she is receptive (0/1), pregnancy status (0/1) and lactation status (0/1). When the female is pregnant, we track time since conception (τ_p). Equations 1–5 in table S1 describe how the derived quantities depend on the core *i*-states variables of age and reserve density.
Besides the specification of the *i*-states, the DEB model describes how the energy flows depend on the *i*-state variables or their derived quantities. The energy flows are the lines connecting the different boxes in figure 1 (main text) and their equations are shown in Table S1 (eqs 6 – 11). The resource ingestion rate is composed of four parts. The first part describes its dependence on resource density by a linear functional response ($\phi_R R$). Here, all the biological quantities (assimilation and conversion efficiencies, resource encounter rates) are captured by R and the multiplication with the scalar ϕ_R only occurs to make the model dimensions correct. Since R and ϕ_R only enter the model through their product ($\phi_R R$) this choice is arbitrary and will not affect model dynamics. The resource density R should be interpreted as the amount of assimilated energy per unit of volume, while the product $\phi_R R$ is the amount of assimilated energy acquired per day per unit of $S^{2/3}$. The second part of I_R describes the scaling of resource ingestion with structural whale mass to the two-thirds power and the product $\phi_R R S^{2/3}$ hence accounts for the resource assimilation rate per whale individual. The third part is the first fraction in eq. (6) and discounts resource assimilation based on the body condition $\frac{F}{W}$. This is a sigmoidal decreasing function of $\frac{F}{W}$ and equals 0.5 at a body condition of ρ. The steepness is controlled by parameter η. The last component of I_R consists of the age-dependency in resource assimilation, which increases from 0 at birth and asymptotically approaches 1 with increasing age. The age at which this function equals 0.5 is controlled by parameter T_R, while the non-linearity of the age-dependency is determined by γ.
Compared to the resource assimilation rate, the milk assimilation rate I_L depends in a similar way on a lactation scalar (ϕ_L), structural size ($S^{2/3}$), body condition ($\frac{F}{W}$) and age of the calf, although the age-dependency takes a different form. Milk assimilation rate is not discounted for calf age during the first year of lactation. Beyond the first year the age-dependency term models an increasing discounting factor with increasing age, up until the age at weaning where the milk assimilation rate becomes zero. The non-linearity of this component is controlled by parameter ξ_c. In addition, milk assimilation rate also depends on the body

condition of the female, as represented by the first term in square brackets in eq. (7). Here, the index m indicates the variable belongs to the female. This factor ensures that milk assimilation becomes zero when body condition of the female hits the starvation threshold ρ_s, while milk assimilation equals 1 when female's body condition equals target body condition ρ. The non-linearity in the decreasing milk supply with decreasing female body condition is controlled by parameter ξ_m.

The different forms of energy expenditure are denoted by C_i and shown in Table S1 eqs. (8-11). Field metabolic costs (eq. 8) are proportional to the ¾–power function of maintenance body weight W_M, following (Kleiber 1975). As discussed in the main text, maintenance body weight discounts for the lower contribution of reserve density to metabolic rate. The costs of growth (eq. 9) follows from the derivative of structural mass with respect to age $\left(\frac{dS(l(a))}{da}\right)$, multiplied by the energetic costs of growing one unit of structural mass (σ_G). Similarly, the costs of growing a foetus are proportional to the derivative of structural mass of the foetus with respect to time since conception $\left(\frac{dS\left(l_p(\tau_p)\right)}{d\tau_p}\right)$, again with proportionality constant σ_G (eq. 10, table S1). The function C_p only covers the structural growth costs of the foetus, while the maintenance costs of the growing foetus are incorporated in the maintenance body weight of the pregnant female directly. Finally, lactation costs eq. (11) are equal to the milk assimilation rate of the calf, but corrected for the efficiency of lactation σ_L. Here, the index c indicates that a variable belongs to the calf.

The three types of age-dependent mortality were captured by the eq. (12) in table S1. This equation was fitted to data of (Bloch et al. 1993*a*) and provide an equal fit to an equation that describes the three forms of age-dependent mortality as separate terms, but required an additional parameter. Starvation mortality only applies when body condition falls below the starvation threshold ρ_s and increases with decreasing body condition (eq. 13). The scaling of this increase is determined by parameter μ_s.

The pregnancy threshold uses the amount of reserves that is required to produce a newly born calf $F_{neonate}$. This quantity is composed of two components (eq. 14). The term $\frac{\sigma_G \omega_1 {l_b}^{\omega_2}}{\epsilon^-}$ accounts for the growth costs of the structural mass of the foetus, express in reserve density of the female (division by ϵ^-). The term $\frac{\rho_s \omega_1 {l_b}^{\omega_2}}{(1-\rho_s)}$ equals the amount of reserves that the female transfers to the calf at birth. This quantity is such that the body condition of the calf at birth is equal to the starvation threshold.

The last equation in table S1 describes how the seasonally varying resource density is modelled. For this we use a cosine function such that resource density equals the yearly mean resource density at the start of each year (t = 0, 365, etc) and increases. This corresponds to spring which is when we assume the focal female is initiated.

Model Parameters

Most model parameters are derived from the international research programme on Northeast Atlantic long-finned pilot whales off the Faroe Islands, which was conducted between July 1986 and July 1988 (Bloch et al. 1993*b*). The year-round drive-fisheries on the Faroe Islands resulted in detailed information on age and growth parameters (Bloch et al. 1993*a*), reproductive parameters (Martin and Rothery 1993) and bioenergetic parameters (Lockyer 1993) of a large number of pilot whales (n > 3000). Some parameter values could not be derived directly from sources (*e.g.* lactation scalar ϕ_L) and these were based on reasonable biological

assumptions and the values of other parameters. All model parameters with reference to the sources used in their derivation are listed in Table S2.
Estimates of gestation and lactation periods are given by (Martin and Rothery 1993) and amount to 12 months (365 days) and 40.2 months (1223 days), respectively. (Lockyer 1993) notes that in the first year of life calves are solely dependent on milk, which gives $T_N = 365$. The duration of the receptive period was calculated by assuming that ovulation occurs once per year and has a chance of pregnancy of 82%. This latter chance is derived from the ratio between the inter-ovulation interval and the interval-birth interval (4.17 : 5.1, as reported by (Martin and Rothery 1993)). This leads to a receptive period of $\frac{365}{0.82} = 445$ days. Estimates for the increase in resource feeding efficiency with age (T_R and γ) are not available and we adopt $T_R = 500$ and $\gamma = 2$. With these values, the resource feeding efficiency increases rapidly at first, equals ~ 86% per cent at weaning age and asymptotically approaches 100%.
((Bloch et al. 1993*a*), their Table 7) report several estimates for length at birth and total weight at birth and we adopt their best estimates of $l_b = 177$ cm and $W_b = 75$ kg. Mean length-at-age data in ((Bloch et al. 1993*a*), their Table 10) is used to fit parameters l_∞ and k. In the fitting procedure, its assumed that the reported ages indicate the beginning of the age classes, which implies that the true mean ages are 0.5 years later. This age-transformation resulted in a satisfactory fit of a non-linear regression with parameters $l_\infty = 450$ and $k = 0.00045$, while fixing $l_b = 177$.
Energy densities for pilot whales at different ages as reported by (Lockyer 1993) were used to estimate the length-structural mass relationship parameters ω_1 and ω_2 and target and starvation body condition parameters ρ and ρ_s. In this derivation we use lipid proportion as an indication of the percentage of reserve density of an individual. The fact that a part of the lipid content of an individual has a structural origin and cannot be mobilized without compromising survival is accounted for by setting the starvation threshold $\rho_s > 0$. Lipid proportion for calves are around 17% (Lockyer 1993), which makes structural mass at birth $S_b = 75 \cdot (1 - 0.17) = 62$ kg. Ultimate body weight is reported by (Bloch et al. 1993*a*) as $W_\infty = 1320$ kg for individuals with $l_\infty = 512$ cm. According to (Lockyer 1993), lipid content of these individuals is around 25%, so by a similar calculation $S_\infty = 990$ kg. This leads to a length-structural mass scaling exponent of $\omega_1 = \ln\left(\frac{S_\infty}{S_b}\right)/\ln\left(\frac{l_\infty}{l_b}\right) = 2.6$.
Consequently, the length-structural mass scaling constant equals $\omega_2 = 8.5 \cdot 10^{-5}$. A large proportion of lipid content of calves (17%) probably belongs to structural mass and cannot be used as energy reserve without endangering life. Based on this we adopt $\rho_s = 0.15$. This corresponds well to the observation that most pilot whales of Faroese population have a body condition in the range 0.14 – 0.23 (Lockyer 1993). Since modelled reserve density equilibrates below the target reserve threshold, we adopt $\rho = 0.30$ and $\eta = 15$.
Compared to the maintenance costs for structural mass, the maintenance costs of reserves are lower per unit body mass. This relative discounting is quantified with parameter θ_F. DEB theory argues that fat reserves do not require maintenance (Kooijman 2010), which implies that $\theta_F = 0$. While the amount of basal metabolic costs of reserves might be limited, reserves can increase field metabolic costs by increasing energetic costs of locomotion and activity. This holds especially for marine mammals, in which large fat reserves can increase drag. We therefore adopt the conservative estimate of $\theta_F = 0.2$. Although maintenance costs of foetal mass might be lower per unit mass than maintenance costs of structural mass, foetal maintenance also includes costs for the placenta as well as increased metabolic costs for the mother due to increased drag and activity costs. Consequently, no discounting for foetal maintenance was applied.
Field metabolic maintenance rate follows Kleiber's relationship (Kleiber 1975). The scalar of this relationship (σ_M) was set to 0.75. This values approximately represents a 2.5 multiple of

basal metabolic rate (Lockyer 1993). Costs of growth in structural mass (represented by σ_G) includes both growth overheads and the energy assembled in the newly synthesized biomass. We derive an estimate for σ_G by combining (Brody 1968) equation for the heat of gestation ($Q_G = 4400W(0)^{1.2}$ in kCal) with energy densities of pilot whales as reported by (Lockyer 1993). Heat of gestation for a 75 kg neonate amounts to 3274 MJ. This includes the foetal maintenance metabolic rate during the gestation period, which equals $\int_0^{T_P} \sigma_M \left(\omega_1 \left(l_b \frac{\tau_p}{T_G}\right)^{\omega_2}\right)^{0.75} d\tau_c = 1987$ MJ. Energy content of a 75 kg neonate is estimated to be 7.95 · 75 · 1.25 = 745 MJ, when accounting for a placenta that adds 25% to the neonate mass and with 7.95 MJ · kg^{-1} being the energy density of foetus and placenta at birth(Lockyer 1993). This implies a growth efficiency of 745 / (3274 – 1987 + 745) = 0.366. Pilot whales calves have a considerably higher energy density of 10.1 MJ · kg^{-1} (Lockyer 1993), which results in $\sigma_G = 27.4$ MJ · kg^{-1}. Since the heat of gestation is likely to be an underestimate of the true costs of gestation we settle for a value of $\sigma_G = 30$ MJ · kg^{-1}.
The conversion efficiency parameter σ_L controls both the assimilation efficiency of milk by calves and the efficiency at which mother produce milk from reserves. (Lockyer 1993) notes that efficiency of milk assimilation is 95% and that mammary gland efficiency of milk production is 90%. Combining these estimates yields a value of $\sigma_L = 0.86$.
The lactation scalar ϕ_L was parameterized such that the amount of energy expended in the first year of life (maintenance and growth costs) can be completely covered by milk suckling, which is reasonable for pilot whales (Lockyer 1993). Energy expended on maintenance during the first year follows from solving the integral: $\int_0^{365} \sigma_M \left[\left(1 + \theta_F \frac{\rho}{1-\rho}\right) \omega_1 l(a)^{\omega_2}\right]^{0.75} da = 7808$ MJ, in which it is assumed that $F/W = \rho$ and that $l(a)$ follows eq. 2 in (table S1). Structural growth during the first year equals 41 kg and corresponding growth costs amount to 1230 MJ. If milk assimilation covers all these expenses then, assuming $F/W = \rho$ for both mother and calf, the milk ingestion rate function I_L (table S1) evaluates to $9038/365 = \phi_L \cdot S^{2/3} \cdot 0.5$. Using an average structural mass of the calf in the first year of $S = \left(\int_0^{365} \omega_1 l(a)^{\omega_2}\, da\right)/365 = 80.5$ kg, gives $\phi_L = 2.7$.
Parameters describing the efficiency of anabolic and catabolic reserve dynamics (ϵ^+ and ϵ^-) were set to 55 MJ · kg^{-1} and 35 MJ · kg^{-1}, respectively. The efficiency of catabolism closely relates to the energy density of fat, which was reported as 40 MJ · kg^{-1} (Lockyer 1993). Applying some efficiency of anabolic conversion leads to the value of 35 MJ · kg^{-1}. Anabolic conversion is considered less efficient and we hence set ϵ^+ to 55 MJ · kg^{-1}.
The parameters ξ_c and ξ_m describe the non-linearity of milk assimilation with calf age and female body condition, respectively. Empirical estimates for these parameters are unlikely to exists, especially specifically for pilot whales. We therefore choose these parameters such that their functions reflect the biological response in a qualitative manner. The parameter ξ_m described how milk supply of the female depends on her body condition and is set to -2, to simulate a decline in the rate of milk provisioning that decreases with decreasing body condition of the mother. The parameter ξ_c controls the steepness of the decrease in milk assimilation rate with increase age of the calf. A value of $\xi_c = 0.9$ ensures that milk suckling decreases with an increasing rate as the calf ages.
Mortality rate parameters are derived from (Bloch et al. 1993*a*), who fit a survivorship curve to an age-frequency plot of Pilot Whales from the Faroe Islands (*n* = 1.482 (Bloch et al. 1993*a*), their figure 3) and present age-specific survival estimates based on the method of (Barlow and Boveng 1991). We use these age-specific survival estimates (P_a) to calculate the age-specific mortality rate as $z_a = -\ln(P_a)$. Subsequently, we fit the mortality rate function

in eq. (12) to the age-specific mortality rates z_a to obtain the estimates of the parameters α_1, α_2, β_1 and β_2 as shown in table S2. We set μ_s to 0.2, which implies a starvation mortality rate of 0.1 day^{-1} for an individual with a body condition of 10% and (ignoring age-dependent mortality) a 50% survival over a period of one week of starvation if body condition remains at 10%.

Table S1: Model equations

Function	Equation	Description	Eq. no
$l_p(\tau_p)$	$l_b \frac{\tau_p}{T_P}, \quad 0 \le \tau_p \le T_P$	Length-age relationship of foetus	(1)
$l(a)$	$l_\infty - (l_\infty - l_b)e^{-ka}$	Von Bertalanffy growth in structural mass	(2)
$S(l)$	$\omega_1 l^{\omega_2}$	Structural mass-length relationship	(3)
$W(S,F,\tau_p)$	$\begin{cases} S+F+S\left(l_p(\tau_p)\right) & \text{pregnant} \\ S+F & \text{otherwise} \end{cases}$	Total weight of an individual	(4)
$W_M(S,F,\tau_p)$	$\begin{cases} S+\theta_F F+S\left(l_p(\tau_p)\right) & \text{pregnant} \\ S+\theta_F F & \text{otherwise} \end{cases}$	Maintenance weight of an individual	(5)
$I_R(a,R,S,F,W)$	$\phi_R R\, S^{2/3} \frac{1}{1+e^{-\eta(\rho W/F-1)}} \frac{a^\gamma}{T_R^\gamma + a^\gamma}$	Energy assimilation rate from resource feeding	(6)
$I_L(a,S,F,W,F_m,W_m)$	$\phi_L S^{2/3} \left[\frac{(1-\xi_m)(F_m-\rho_s W_m)}{(\rho-\rho_s)W_m-\xi_m(F_m-\rho_s W_m)}\right]_+ \cdot \frac{1}{1+e^{-\eta(\rho W/F-1)}} \min\left(1, \left[\frac{1-\frac{a-T_N}{T_L-T_N}}{1-\xi_c\frac{a-T_N}{T_L-T_N}}\right]_+\right)$	Energy assimilation rate from milk	(7)
$C_M(W_M)$	$\sigma_M W_M^{3/4}$	Field metabolic costs	(8)
$C_G(l)$	$\sigma_G \omega_1 k(l_\infty - l)\omega_2 l^{\omega_2-1}$	Somatic growth costs	(9)
$C_P(\tau_p)$	$\sigma_G \omega_1 \omega_2 \left(\frac{l_b}{T_P}\right)^{\omega_2} \tau_p{}^{\omega_2-1}, \quad 0 \le \tau_p \le T_P$	Pregnancy costs	(10)
$C_L(F,W,a_c,S_c,F_c,W_c)$	$I_L(a_c,S_c,F_c,W_c,F,W)/\sigma_L$	Lactation costs	(11)
$D(a)$	$\alpha_1 e^{-\beta_1 a} + \alpha_2 e^{\beta_2 a}$	Mortality rate	(12)

$D_s(F,W)$	$\mu_s\left(\frac{\rho_s W}{F}-1\right), \qquad F<\rho_s W$	Starvation mortality rate	(13)
$F_{neonate}$	$\frac{\sigma_G \omega_1 {l_b}^{\omega_2}}{\epsilon^-}+\frac{\rho_s \omega_1 {l_b}^{\omega_2}}{(1-\rho_s)}$	Amount of fat reserves required to produce body weight of one neonate	(14)
	$F>\rho_s W+F_{neonate}$	Pregnancy threshold	(15)
R	$\bar{R}\left(1.0-A\cos\left(\frac{2\pi(t+91.25)}{365}\right)\right)$	Resource dynamics	(16)

Table S2: Model Parameters

Symbol	Unit	Value	Description	Source
T_P	day	365	Gestation period	Martin & Rothery 1993
T_L	day	1223	Lactation period (age at weaning)	Martin & Rothery 1993
T_N	day	365	Age at which milk consumption starts to decrease	–
T_R	day	500	Age at which resource foraging is 50%	–
T_D	day	445	Receptive period before onset of pregnancy	Martin & Rothery 1993
l_b	cm	177	Length at birth	Martin & Rothery 1993
l_∞	cm	450	Ultimate length in Von Bertalanffy Growth Curve	Bloch et al. 1993; this study
k	day^{-1}	0.00045	Von Bertalanffy growth rate	Bloch et al. 1993; this study
ω_1	$kg \cdot cm^{-\omega_2}$	$8.5 \cdot 10^{-5}$	Mass-length scaling constant	Bloch et al. 1993; this study
ω_2	–	2.6	Mass-length scaling exponent	Bloch et al. 1993; this study
θ_F	–	0.2	Relative maintenance costs of reserves	–
ρ	–	0.30	Target ratio of reserves to total weight	Lockyer 1993
ρ_s	–	0.15	Reserve threshold onset starvation mortality	Lockyer 1993
ϕ_R	$m^3 \cdot kg^{-2/3} \cdot day^{-1}$	1.0	Resource encounter rate scalar	–
ϕ_L	$MJ \cdot kg^{-2/3} \cdot day^{-1}$	2.7	Energy provisioning rate through lactation scalar	Lockyer 1993; this study
η	–	15	Steepness of assimilation response around target reserves ratio	–
γ	–	2	Shape parameter of resource assimilation-age response	–
ξ_m	–	–2.0	Non-linearity in female reserve ratio-milk provisioning relation	–
ξ_c	–	0.9	Non-linearity in milk assimilation-calve age relation	–

σ_M	MJ·kg$^{-3/4}$·day^{-1}	0.75	Field metabolic maintenance scalar	Lockyer 1993
σ_G	MJ·kg^{-1}	30	Energetic costs per unit structural mass growth	this study
σ_L	–	0.86	Lactation conversion efficiency	Lockyer 1993
α_1	day^{-1}	4.01·10^{-4}	Mortality parameter	Bloch et al. 1993; this study
β_1	day^{-1}	5.82·10^{-4}	Mortality parameter	Bloch et al. 1993; this study
α_2	day^{-1}	6.04·10^{-6}	Mortality parameter	Bloch et al. 1993; this study
β_2	day^{-1}	3.01·10^{-4}	Mortality parameter	Bloch et al. 1993; this study
μ_s	day^{-1}	0.2	Starvation mortality scalar	–
ε^+	MJ·kg^{-1}	55	Anabolic reserves conversion efficiency	–
ε^-	MJ·kg^{-1}	35	Catabolic reserves conversion efficiency	Lockyer 1993
$\bar{R}$	MJ·m^{-3}	1.6 – 3.0	Mean annual resource density	–
A	–	0, 0.15, 0.3, 0.45	Relative amplitude of seasonal resource fluctuation	–

References

Barlow, J., and P. Boveng. 1991. Modeling Age-Specific Mortality for Marine Mammal Populations. Marine Mammal Science 7:50–65.

Bloch, D., C. Lockyer, and M. Zachariassen. 1993*a*. Age and Growth Parameters of the Long-Finned Pilot Whale off the Faroe Islands. Biology of Northern Hemisphere Pilot Whales 163–207.

Bloch, D., G. Desportes, R. Mouritsen, S. Skaaning, and E. Stefansson. 1993*b*. An Introduction to Studies of the Ecology and Status of the Long-finned Pilot Whale (*Globicephala melas*) off the Faroe Island, 1986 – 1988. Biology of Northern Hemisphere Pilot Whales 1–32.

Brody, S. 1968. Bioenergetics and Growth (Vol. 13). Hafner Publishing Co., New York.

Kleiber, M. 1975. The fire of life: an introduction to animal energetics. R.E. Krieger Pub. Co., Huntington, N.Y.

Kooijman, S. A. L. M. 2010. Dynamic Energy Budget theory for metabolic organisation (Third edition.). Cambridge University Press, Cambridge, UK.

Lockyer, C. 1993. Seasonal Changes in Body Fat Condition of Northeast Atlantic Pilot Whales, and their Biological Significance. Biology of Northern Hemisphere Pilot Whales 325–350.

Martin, A. R., and P. Rothery. 1993. Reproductive Parameters of Female Long-Finned Pilot Whales (*Globicephala melas*) Around the Faroe Islands. Biology of Northern Hemisphere Pilot Whales 263–304.